This is a post-print (peer-reviewed, corrected) version of: Harishidayat D, Omosanya KO, Johansen SE, Eruteya OE, Niyazi Y (2018). Morphometric analysis of sediment conduits on a bathymetric high: implications for palaeoenvironment and hydrocarbon prospectivity. Basin Res 30:1015–1041. https://doi.org/10.1111/bre.12291

Morphometric analysis of sediment conduits on a bathymetric high: implications for paleoenvironment and hydrocarbon prospectivity

Dicky Harishidayat[1*], Kamaldeen Olakunle Omosanya[1], Ståle Emil Johansen[1], Ovie Emmanuel Eruteya[2], Yakufu Niyazi[3]

[1]Department of Geoscience and Petroleum Engineering, Norwegian University of Science and Technology, Trondheim

[2]Department of Earth Sciences, University of Geneva, Geneva

[3]Dr. Moses Straus Department of Marine Geosciences, Leon H. Charney School of Marine Sciences, University of Haifa, Haifa

*Corresponding author: dicky.hidayat@ntnu.no

Abstract

Canyons and other sediment conduits are important components of the deep-water environment and are the main pathways for sediment transport from the shelf to the basin floor. Using 3D and 2D seismic reflection data, seismic facies and statistical-morphometric analyses, this study showed the architectural evolution of five canyons, two slide scars and four gullies on the southern part of the Loppa High, Barents Sea. Morphometric parameters such as thalweg depth (lowest point on a conduit's base), wall depth (middle point), height, width and base width, sinuosity, thalweg gradient, aspect ratio (width/height) and cross-sectional area of the conduits were measured at intervals of 250 m perpendicular to the conduits' pathways. Our results show that the canyons and slide scars in the study area widen down slope, whereas the gullies are narrow and short with uniform widths. The sediment conduits in the study area evolved in three stages. The first stage is correlated with a time when erosion and bypass were dominant in the conduits, and sediment transferred to the basin in the south. The second stage occurred when basin subsidence was prevalent, and a widespread fine-grained sequence was deposited as a drape blanketing the canyons and other conduits. A final stage occurred when uplift and glacial erosion configured the entire southern Loppa High into an area of denudation. Our work demonstrates that the morphometric parameters of the canyons, slide scars and gullies generally have increasing linear trends with down-slope distance, irrespective of their geometries. The morphometric analysis of the sediment conduits in the study area has wider applications for understanding depositional processes, reservoir distribution, and petroleum prospectivity in frontier basins.

Keywords: sedimentology, seismic geomorphology, morphometry, paleoenvironment, Loppa High, canyon, gully, slide scar, Barents Sea, hydrocarbon prospectivity

1.0 Introduction

Sediment conduits such as canyons, channels, and gullies are important components of the deep-water depositional system (Stow & Mayall 2000; Normark & Carlson 2003; Posamentier & Kolla 2003; Mayall *et al.* 2006; Posamentier & Walker 2006; Shanmugam 2006; Gamboa *et al.* 2012). They represent the principal pathways for transporting sediments from the continental shelves to the basin floor (Shepard 1963; Shepard & Marshall 1973; Mutti & Normark 1991; Normark *et al.* 1993; Stow & Mayall 2000; Normark & Carlson 2003; Flint & Hodgson 2005; Posamentier & Walker 2006; Deptuck *et al.* 2007; Kolla 2007; Fildani 2017). In the last few decades, their architectures, morphometries and the processes leading to their development have been investigated in different deep-water depositional systems and geologic settings from marine geophysical data (Friend 1983; Mutti & Normark 1987; Miall 1989; Clark & Pickering 1996; Deptuck *et al.* 2007; Jobe *et al.* 2011; Qin *et al.* 2016). High-quality marine three-dimensional (3-D) seismic reflection data have allowed the true dimensionalities and morphometric characters of several sediment conduits to be imaged and observed. Where proper acquisition parameters and line directions (e.g. perpendicular to the sediment conduits) are used, two-dimensional (2-D) seismic reflection data can also potentially capture the true geometries of these sediment conduits (Omosanya *et al.* 2016). However, the interpretation of canyons and other sediment conduits from seismic reflection data poses several challenges that are related to variations in the conduits' morphometries, limitations in seismic resolution, line spacing, internal compositional variations, and the influences of external geologic processes (Deptuck *et al.* 2007; Gamboa & Alves 2015; Qin *et al.* 2016; Ortiz-Karpf *et al.* 2017).

Several studies indicate that the dominant controls on sediment distributions in basins can be inferred from the processes and resultant stratigraphic architectures of the deposits (Clark & Pickering 1996; Deptuck *et al.* 2008; Paquet *et al.* 2009; Covault & Graham 2010). While a cornucopia of stratigraphic architectures and compositions of canyons and other sediment conduits has been documented, a quantitative description of their morphometric aspects (especially focused on the character of the base of the sediment conduits) is relatively unexplored. This provides the impetus to propose and accomplish a holistic description of the geometries of the sediment conduits and to provide an exhaustive analysis of their controlling factors. This study aims to a) investigate the seismic stratigraphic architectures and depositional elements of several types of sediment conduits and their filling deposits, b) understand their scales and morphometries and c) evaluate the processes that create canyons and other sediment conduits on a bathymetric high. To achieve these aims, we have used a case study area in the southern part of the Loppa High, Barents Sea (Figure 1a). The canyons, gullies and slide scars in this area acted as conduits for the transport of Triassic-Cretaceous

strata, which were deposited as submarine fans in the Northern Hammerfest Basin (Wood *et al.* 1989; Faleide *et al.* 1993; Marín *et al.* 2016).

The southern part of the Loppa High is a natural laboratory to study the interplays among geodynamic evolution, erosion, and sediment transport due to its complex geodynamic evolution (Faleide *et al.* 1993; Indrevær *et al.* 2016; Marín *et al.* 2016). Additionally, the high quality of the seismic data allowed detailed mapping of the bases of the canyon systems. In this study, we have applied a statistical approach to the study of canyons, gullies and slide scars, making it possible to provide detailed insights into their architectures and stratigraphic variability. Our study provides important information that is useful for hydrocarbon exploration activities in the study area and other frontier basins, especially on bathymetric high systems. The paper starts with an analysis of seismic facies (depositional and architectural elements) and follows-up with thorough morphometric descriptions of the different types of sediment conduits from a statistical perspective. The results of the development and implications of the sediment conduits' morphologies for the paleoenvironment and hydrocarbon prospectivity are discussed.

2.0 Geological setting

Tectonic rifting and uplift as well as short- and long-term local and regional sea-level variations have determined the depositional history of the Barents Sea from the Late Palaeozoic to the Early Cenozoic (Wood *et al.* 1989; Faleide *et al.* 1993; Worsley 2008). Due to the complex interplay of several geologic processes, the Barents Sea has evolved into a number of sub-basins and topographic highs with significant structural relief from the Svalbard Platform to the Norwegian coast (Doré 1995). Compressive tectonics forming the Ural Mountains to the east began in the Late Palaeozoic and ended with continental collision in the Early Mesozoic. These older tectonic events were followed by the proto-Atlantic extension in the west, opening of the Euramerican Basin to the north, and finally by transpression, transtension, and opening of the Norwegian-Greenland Sea in the Cenozoic (Faleide *et al.* 1993; Doré 1995; Worsley 2008).

The study area encompasses the southern part of the Loppa High, which is a NE-SW oriented structural feature in the southwestern Barents Sea (Figure 1a). To the south, the Loppa High is separated from the Hammerfest Basin by the Asterias Fault Complex, while to the west, the Bjørnøyrenna and Ringvassøy-Loppa Fault Complex delimits the Loppa High from the Bjørnøya and Tromsø Basins (Figure 1a). The Loppa High grades into the Bjarmeland Platform to the east. Hence, it forms a triangular basement block with a steep, easterly-dipping eastern flank and a fault-bounded western flank, which has undergone several phases of uplift,

subsidence, tilting, and erosion (Wood *et al.* 1989; Faleide *et al.* 1993; Faleide *et al.* 1996; Henriksen *et al.* 2011a; Henriksen *et al.* 2011b).

The present configuration of the Loppa High is a result of Late Jurassic to Early Cretaceous tectonism, but its shape was defined by earlier mid-Carboniferous rifting that was followed by tectonic uplift and tilting of the flank during the Late Permian and Early Triassic (Gabrielsen *et al.* 1990). During the Late Triassic to Early Jurassic, the Loppa High acted as a depocentre before it underwent another phase of uplift in the Early Cretaceous (Henriksen *et al.* 2011b). Renewed faulting and uplift of the Loppa High during the Late Jurassic to Early Cretaceous led to erosion of the Jurassic and Triassic sediments over the high. Erosion at that time is demonstrated by deeply cutting valleys, through which sediment was transported and deposited as submarine fans in the basins to the south and west (Wood *et al.* 1989; Faleide *et al.* 1993; Richardsen *et al.* 1993). In addition, the global sea-level curve shows a trend of relative sea-level fall during those times (Figure 1b). On-lapping reflections from the Hammerfest Basin onto the Loppa High show that the Asterias Fault complex was tectonically active during the Aptian-Albian (Faleide *et al.* 1993).

In the Late Pliocene-Pleistocene, the Barents Shelf underwent repeated glaciations that were followed by major erosion and uplift (Faleide *et al.* 1993; Mattos *et al.* 2016; Zieba *et al.* 2017). The late uplift and erosion probably began earlier in the Late Cenozoic, and the net erosion is estimated to have been approximately 1000–1500 m in the Loppa High area (Henriksen *et al.* 2011a). Due to that erosion, the Jurassic and younger sediments are not well preserved (Figure 1c) on the present day Loppa High (Wood *et al.* 1989; Faleide *et al.* 1993). The Jurassic and later geological evolution of the Loppa High is therefore difficult to interpret. However, remnants of the Jurassic and younger sediments along the SE flank of the Loppa High may still be preserved.

3.0 Definition of sediment conduit terminology

The term canyon as used herein refers to relatively steep gradient, steep-walled and deep incisions cut into both bedrock (continental shelf at the shelf or slope break) as well as partially indurated substrates that are characterized by V-shaped transverse profiles that indent the shelf and uppermost slope and were formed by submarine erosive processes (Shepard 1965; Shepard 1972; Normark *et al.* 1993; Normark & Carlson 2003; Posamentier & Walker 2006; Covault 2011; Harris & Whiteway 2011; Talling 2014; Fildani 2017).

A slide scar is a major erosional feature produced by shelf edge slope failure (Normark *et al.* 1993; Haflidason *et al.* 2004) or sediment released during a single event of retrogressive sliding

(Bøe *et al.* 2000). These features can form in extremely short periods of geological time (thousands of years or less) and originate from retrogressive slumping until the slope re-establishes a stable profile (Normark *et al.* 1993). Slide scars were probably initiated along a bedding-parallel weak horizon but propagated upward at points where downslope driving stresses decreased or resisting forces increased (Lee & Stow 2007). Slide scars that developed on continental margins by slope failure may evolve into channels through which sediments are transported downslope by either mass wasting, turbidity currents or both (Farre *et al.* 1983; May *et al.* 1983; Klaus & Taylor 1991; Roep & Fortuin 1996; Stow *et al.* 1996; Haflidason *et al.* 2004).

A gully is a small-scale conduit incision (10s m deep) on the slope (between the shelf edge and the toe-of-slope) that generally is of low relief, straight, and does not reach base-level (Field *et al.* 1999; Stow & Mayall 2000; Posamentier & Walker 2006; Shanmugam 2006; Lonergan *et al.* 2013; Talling 2014; Prélat *et al.* 2015; Shumaker *et al.* 2016; Amblas *et al.* 2018). Gullies can be distinguished from channels by their spatial distributions (gullies commonly occur in evenly-spaced groups), where the gully heads incise the shelf edge or upper continental slope. The width/depth ratio (W/D) is a dimensionless ratio that provides an indication of gully shape, and their stacking patterns are dominantly aggradational (Gales *et al.* 2013; Lonergan *et al.* 2013).

4.0 Data and approach

4.1 Seismic dataset

The primary dataset for this study consists of full-stack, 3-D and 2-D seismic reflection data with wireline logs from ten exploration wellbores (Figure 1a). The 3-D seismic data include two cubes, SG9803 and OMV09M01. The SG9803 cube has a line spacing of 12.5 m and a vertical sampling rate of 4 milliseconds. The dominant frequency for the 3-D seismic survey in the study area is 25 Hz, with an average velocity of 2600 m/s in the interval of interest (450 – 1250 milliseconds). Hence, the seismic cube has a vertical resolution of 26 m. The data are zero-phased and displayed in Society of Geophysicists (SEG) normal polarity, where a positive seismic amplitude or white reflection represents an increase in acoustic impedance (Figure 1b). Decreasing acoustic impedances are shown as black reflections or troughs. Similarly, the OMV09M01 cube has a line spacing of 12.5 m and a vertical sampling of 4 ms, and the inlines were acquired at a 0° rotation from north. The dominant frequency in the focus area is 30 Hz, and the average velocity is 2200 m/s, giving a vertical resolution of 18.3 m in the interval of interest (600 – 1000 milliseconds). The OMV09M01 cube is also zero-phased and displayed with SEG normal polarity as for the SG9803 cube. Additionally, sixty-three 2-D seismic lines

from seven 2-D seismic surveys are available for this study (Figure 1a). Most of the 2-D seismic lines have vertical sampling intervals of 4 ms and are oriented in several directions, as shown in Figure 1a. The phases, polarities and dominant frequencies of the 2-D seismic lines are similar to those of the 3-D data (zero-phased, SEG normal polarity and 30 Hz). The quality of 2-D seismic data in the target interval is considered to be good.

4.2 Wellbore data

Ten exploration wellbores were used in this study in addition to the seismic data (Figure 1a). Unfortunately, none of them penetrated the canyons and sediment conduits in the southern part of the Loppa High. The average total-depth for these exploration wellbores is 2500 m, with the oldest penetrated formation being the Ugle Formation (Late Carboniferous) in wellbore 7220/11-1, whereas most of the wells penetrated the Late Triassic Fruholmen, Snadd, and Tubåen Formations. Standard wireline logs such as gamma ray (GR), deep resistivity (RDEP), neutron (NEU), density (DEN), and sonic (DT) were used for the interpretation of lithology and as checkshot data for the seismic well-tie process. The seismic well-tie process was undertaken using checkshot, density and sonic log data from the boreholes in order to relate the seismic horizons to their appropriate depths and formation stratigraphy. The seismic well-tie process encountered some challenges in the shallow interval as the checkshot and sonic data are of inferior quality or missing. A further interpretation of the lithology utilized conventional cores and cutting descriptions from the mud logs. Information on formation stratigraphy, name, and ages was obtained from Gradstein *et al.* (2010).

4.3 Seismic interpretation

Faults and five horizons were interpreted using Schlumberger's Petrel® software. The horizons (Figure 1b) include the seabed (H5), top of the Kolje Formation (H4), base of the sediment conduit system (Erosional surface: H3), top of the Snadd Formation (H2), and top of the Kobbe Formation (H1). Seismic time to depth conversion was performed using a simple velocity model (interval velocity) that mainly integrated the time-depth (T-D) relationship from the seismic to well-tie process within the interpreted horizons. This process is important to calculate the vertical morphometric factors in depth and not in time.

The seismic facies analyses consisted of architectural (erosional surface) and depositional (filling deposit) element analyses to characterize the canyons, gullies and slide scars in the study area (Figure 2). In general, the erosional surfaces of the conduits consist of the bases, walls and flanks of the incisions (Figure 2). A base is a low area on the erosional surface of a sediment conduit. The lowest point of a conduit is called the thalweg (for canyons and gullies)

and LPS (Lowest Point of Slide scar). A wall is the steep-sided area on an erosional surface, and a flank is the area outside the overspill point of a sediment conduit. In addition, a canyon terrace is defined as a topographically flat area between a thalweg and wall (Figure 2). These architectural elements of the erosional surfaces of sediment conduits have been defined based on the works of Shepard (1965), Shepard (1972), Goodwin & Prior (1989), Normark *et al.* (1993), Stow *et al.* (1996), Posamentier & Kolla (2003), Babonneau *et al.* (2004), Haflidason *et al.* (2004), Posamentier & Walker (2006), Catterall *et al.* (2010), Tubau *et al.* (2013) and Tubau *et al.* (2015).

Consequently, there are four depositional elements or filling deposits of the sediment conduits in the study area, which are the Conformable Reflection Element (CRE), the Massive Low Amplitude Reflection Element (MLARE), the High Amplitude Reflection Element (HARE) and the scars (Figure 2). The CRE is characterized by draping seismic reflections (Figure 2) that are laterally uniform for long distances (> 20 km), and core data demonstrate that they are comprised largely of clays that mantle the pre-existing topography and are not related to current activity (Jobe *et al.* 2011). MLARE includes parallel and subparallel, low amplitude seismic reflections (Figure 2) that consist of fine grained material suspended into the sediment conduit system (Posamentier & Kolla 2003). HARE as a filling deposit is predominantly located at the base of canyon system and is associated with canyon thalwegs (Figure 2). HARE in the study area consists of high amplitude reflections that are laterally discontinuous (Figure 2) and are interpreted to result from the presence of coarse-grained sediment (Jobe *et al.* 2011). The scars (filling deposits) in the study area are mostly found in the canyon system (Figure 2) and are characterized by discontinuous and isolated reflections (high and low amplitudes) that sit on the upper or middle parts of the canyon walls (sensu Sayago-Gil *et al.* 2008). The scars are products of canyon wall collapse and, as discussed by Völker *et al.* (2012), may be explained either by the (1) absence or presence of weak sediment layers, (2) differences in the activity and geometry of the canyon systems due to tectonic deformation (bends undercutting canyon walls controlled by active thrust ridges) or (3) latitudinal shifts in sediment composition and deposition rate.

The quantitative analysis of the seismic geomorphology of canyons and other sediment conduits in the study area followed the methods proposed by Deptuck *et al.* (2007), Gamboa & Alves (2015), Qin *et al.* (2016) and Hansen *et al.* (2017). Detailed morphological analyses (Figure 3) of sediment conduits were only performed on the 3-D seismic data, whereas the 2-D seismic lines were used for regional correlations of horizons and units (Figures 1a, 4a, and 4c). Morphometric parameters of the canyons, slide scars, and gullies were measured at intervals of 250 m (average) down-dip (the zero points are located in the proximal areas) and

perpendicular to their axis lines (Figure 4). The parameters of importance measured for all these geomorphic features are shown in Figure 3. These are depth from sea level (defined as a middle point of a sediment conduit's walls and the lowest point of the erosional surface), height (defined as the height of sediment conduits from their base to the overspill point), width (defined as the perpendicular width of a sediment conduit and its base) and Cross Sectional Area (CSA; defined as the perpendicular area of a sediment conduit). Furthermore, canyon gradient was calculated based on changes in thalweg depth along the length of a canyon (Deptuck *et al.* 2007; Gamboa & Alves 2015; Qin *et al.* 2016). The gradients for slide scars and gullies were calculated in the same way as for canyons in the study area. All the morphometric parameters are presented in the cross-plot together with the down-sediment conduit distance. In addition, R is the coefficient of correlation that measures the strength and the direction of a linear relationship between two variables on the cross-plot, and R^2 is a coefficient of determination that measures the proportion of the variance (fluctuation) of one variable that is predictable from the other variable on the cross-plot (James *et al.* 2013). The definitions of the proximal, medial and distal areas of the sediment conduit system were based on gradient. Additionally, sinuosity index was measured as a ratio between the length of the lowest point of the erosional surface (thalweg or LPS) and the overall down-system distance for a given section (Wynn *et al.* 2007). Therefore, the detailed sinuosity classification by Reimchen *et al.* (2016) has been used here. The straight conduit systems are defined by sinuosities between 1.0 and 1.05, those for the low sinuosity system are defined as being between 1.05 - 1.2, and those for the high sinuosity system are defined as exceeding 1.2. In addition, the aspect ratios between the widths and heights of the sediment conduit systems are also described.

5.0 Morphological analysis of sediment conduits

Three sediment conduit systems, i.e., canyons, gullies, and slide scars, were investigated within the Late Jurassic-Cretaceous strata in the southern part of the Loppa High (Table 1 and Figure 4a). These conduits are oriented mainly in NW-SE, NE-SW, and E-W directions, reflecting the overall configuration of the Loppa High, i.e., that of a triangular basement block (Figures 1a and 4a). A common attribute of all the conduits is that their bases are erosional and comprise parts of the Triassic Fruholmen and Snadd Formations, which were deposited in fluvial environments (Figures 1b, 2, and 4).

5.1 Canyons

Eight canyons were identified in the study area (Figure 4a), and five of them (located on the 3-D seismic data) were investigated in more detail (Figure 4b). The orientations of the first five

canyons are mainly from NW to SE. The lengths of the canyons vary from approximately 3 km to 13 km, including the tributary canyons. Most of the canyons are V-shaped, with wider canyon-widths at the distal parts of the canyon system (Figure 5). Additionally, most of the canyons have low sinuosities (average sinuosity index of 1.06) at their middle parts and are relatively straight (average sinuosity index of 1.03) at their proximal and distal parts (Table 1 and Figures S1c – S5c). Few of the canyons have tributaries in the proximal or middle parts of the canyon system (Figures 4a, 4b, S2, S4, and S5). In the proximal and middle areas, the canyon gradients are > 0.2°, whereas in the distal areas, the canyon gradients are < 0.2° (Table 1, Figures 6 and S1 - S5).

5.1.1 Depositional elements of the filling deposits

The four main seismic depositional elements identified within the canyons include Conformable Reflection Elements (CREs), High Amplitude Reflection Elements (HAREs), Massive Low Amplitude Reflection Elements (MLAREs), and scars (Figures 2 and 5). Most of the CREs from proximal to distal areas are shown as low to medium amplitude units, whereas the high amplitude CREs are located in the middles of the canyon fill deposits (Figures 2 and 5). The majority of the CREs are canyon fill deposits with folded strata in the middles of the canyons. These folded strata of the CREs are also on-lapping to the edges of the canyons and can be traced with remarkable continuity in the inter-canyon areas (Figure 5). Conversely, the HARE depositional elements in the study area are located at the bases of the canyons and are correlated with the first stage of canyon development, i.e., the erosional phase. The lateral distribution from the proximal to distal areas of the HAREs is continuous and is only discontinuous when faulted (Figures 2 and 5). MLAREs are among those canyon fill deposits that are characterized as having low amplitudes and massive, and in some canyons, they show sub parallel reflections (Figures 2 and 5). Scars in the canyon systems are characterized by discontinuous and isolated reflections that sit on the upper or middle parts of the canyon walls (Figures 2 and 5).

5.1.2 Canyon surface architectural elements

The five elements of the canyon surface architectures observed in the study area include V-shaped canyon-bases (including canyon thalwegs), terraces, canyon-walls and canyon flanks (Figures 2 and 5). The V-shaped canyon bases are the most common canyon surface architecture (Figure 5). Dipping reflections (> 20°) are associated with the V-shaped canyon bases, with the dip angles of the canyon bases decreasing to the proximal parts of the canyons (Figure 6a). In addition, medium to high amplitudes and continuous reflections dominate the canyon bases, whereas canyon base steps are present due to faulting (Figure 5). The terrace

architecture is typified by low to high seismic amplitudes (compared to those from the bases of the canyons) and parallel-subparallel seismic reflections dipping at less than 10° (Figure 5). In some of the canyons, stepped terraces occur due to faulting (Figure 5). Dipping, low to high amplitude reflections (> 30°) characterize the canyon walls, which are continuations of the canyon bases (Figure 5), and in some areas, the canyon walls have discontinuous reflections that indicate sidewall collapses, erosion or faulting of the canyons (Figure 5). Furthermore, the canyon flanks in the proximal and middle parts are relatively flat compared to those in the distal parts of the canyon system (Figure 5). These flanks are parallel-subparallel, have medium to high amplitudes, are faulted and have discontinuous seismic reflections. In some adjacent canyons, one flank can be associated with two different canyons (e.g., Figure 6a).

5.1.3 Quantitative morphometric analysis of canyons

In general, proximal canyons show a V-shaped morphology dominated by steep canyon-walls with terraces, whereas the distal parts have a V-shaped morphology and steep canyon-walls only (Figures 5 and 6a). The canyon thalwegs and walls in the proximal parts of the SE Loppa High have depths ranging from 400 m to 700 m with down dip thalweg gradients that are > 1.1°, whereas they have depths of 750 m to 1250 m with gradients that are < 0.1° in the distal parts of the canyon system (Figure 6b). In the study area, canyon gradients decrease towards the distal parts (Table 1 and Figure 6). The linear correlation between the depths of the canyon thalwegs and walls shows that increases in depth are proportional with increasing down-canyon distances (Figure 6b and Figures S1a – S5a). The canyon heights in the proximal areas are approximately 30 m to 290 m and range from 150 m to 400 m in the distal areas (Table 1 and Figure 6c). The general trend of canyon heights is to increase with down-canyon distance due to the increasing depths of the canyon thalwegs (sensu Mountjoy *et al.* 2009; Brothers *et al.* 2013; Obelcz *et al.* 2014; Tubau *et al.* 2015). Nonlinear correlations exist between down-canyon distance and canyon height for canyons 1, 3 and 5 (Figures S1b, S3b, and S5b). These nonlinear correlations are represented by relatively low values (on average: < 0.6) of the coefficients of correlation and determination (R and R^2, respectively).

The canyon widths in the proximal areas vary from 70 m to 1800 m, whereas the widths range from 900 m to 4500 m in the distal areas (Table 1 and Figure 6d). Canyon base widths in the proximal areas range between 30 m to 150 m, whereas they can vary from 30 m to 1000 m in the distal areas (Table 1 and Figure 6d). In general, the width profiles of the canyons and canyon bases show parallel trends from the proximal to distal areas of the canyon systems. In contrast, the canyons and canyon base widths exhibit no correlation with down-canyon distance, with R and R^2 values of < 0.6 (Table 1, Figure 6d, and Figures S1c – S5c). These low correlations are attributed to the sinuosities of the canyons (Table 1, Figure 6d, and Figures

S1c – S5c) and local canyon-wall failures. Canyon systems in the study area have width to height aspect ratios between 2.6 to 16.3 in their proximal parts and 3 to 14 in their distal parts (Table 1). There is no consistent trend in the aspect ratios of the canyon system in the study area. Furthermore, there are linear trends in the cross-sectional areas of the canyons, with the trends becoming higher in the proximal parts of the canyons. The CSA of canyons in the proximal parts of the Loppa High vary from 0.01 km^2 to 0.50 km^2 and from 0.10 km^2 to 1.8 km^2 in the distal parts (Figure 6e). The R and R^2 values are < 0.6 for the plot of the cross-sectional areas of the canyons against the down-canyon distances. Regarding canyon gradients, medial areas have canyon gradients that are 0.3° (on average). Here, low sinuosity canyons (average sinuosity index of 1.06) with canyon base widths of 100 m to 800 m are present, whereas straight canyons (average sinuosity index of 1.03) mostly dominate the distal parts, where the canyon gradients are 0.1° (Figure 6d). In addition, the ratio of the top and base width of the canyon system in the study area is low (< 0.24).

5.2 Slide scars

Two very wide U-shaped slide scars have been identified within the Late Jurassic-Cretaceous interval in the western part of the study area (Figures 4a and 4b). The slide scars have a NW to SE trend and preserved lengths of approximately 3.75 km (Slide scar 1) and 2.6 km (Slide scar 2). The general sinuosity of the slide scars in the study area is characterized as straight, with a maximum sinuosity value of 1.05 and a minimum value of 1.00 (Table 1).

5.2.1 Depositional elements of the filling deposits

The two main seismic depositional elements of the filling deposits identified in the slide scar system include CREs and MLAREs, i.e., Massive Low Amplitude Reflection Elements (Figure 2). Most of the CREs have low to medium amplitudes and folded strata in the middles of the slide scar fill deposits. The CREs can be traced with remarkable continuity in the inter-slide areas (Figure 7). On the other hand, the MLAREs are low amplitude reflections underlying the CREs and are also representative of slide scar fill deposits (Figure 7).

5.2.2 Slide scar architectural elements

The four elements of the slide scar architecture are U-shaped bases (including the lowest points: LPS), walls and flanks (Figures 2 and 7). The U-shaped bases represent slide escarpment systems marked by long and wide (> 500 m) dipping reflectors (< 10°). Continuous and medium to high amplitude reflections dominate the U-shaped bases and occasionally are abutted by faults (Figure 7). The walls of the slide scars, i.e., continuations of the U-shaped bases, are characterized by long and wide (> 500 m) dipping reflectors (> 10°) with low to high

amplitude reflections (Figures 2 and 7), whereas occasionally the walls of the slide scars have discontinuous reflections due to faulting (Figures 2 and 7). The first set of slide scar flanks is represented by long reflections (> 500 m) that are typified by medium to high amplitudes and are parallel to subparallel with continuous and discontinuous reflections dipping at 0° - 10° (Figure 7). Another type is the stepped flanks that are mostly influenced by a series of normal faults in the study area and are shown as low to high amplitudes and parallel reflections (Figure 7). Furthermore, the slide scar flanks in the proximal and middle parts are relatively steep when compared to those in the distal parts (Figure 7). In the distal parts of the slide scars, one flank can belong to two different slide scars (e.g., Figure 8a).

5.2.3 Quantitative morphometric analysis of slide scars

In terms of slide scar geometry, both slides have very wide U-shaped bases and flanks (> 500 m), with Slide scar 1 having steeply dipping side scar walls (Figure 7). Both the proximal and distal areas of the slide scars are U-shaped and dominated by steep walls with discontinuous, medium to high amplitude reflections (Figure 7). However, the proximal domains of the slide scars have faulted bases. The slide scar gradients decrease towards their distal parts (Table 1 and Figure 8). The depth profiles of the LPS and slide scar walls are divided into three intervals based on changes in depth and slide scar gradient (Table 1, Figures 8a and 8b). The first intervals (proximal areas) show no significant changes in depth and have gradients of 1.3° (Figure 8b). The second intervals (medial areas) show significant changes in depths from 20 m to 50 m and slide scar gradients decreasing from 1.3°–0.5°, whereas the last intervals (distal areas) show significant changes in depths from 20 m to 70 m and gradients decreasing to < 0.3° (Figures 8a and 8b). In general, there are good correlations between LPS and wall depth with down-slide scar distance (Figures 8b, S6a and S7a). This results in high R and R^2 values of 0.99 and 0.98, respectively, for the LPS and 0.93 and 0.86, respectively, for the slide scars' walls (Figures S6a and S7a). Furthermore, the slide scar height profiles in the study area show linear trends with down-slide scar distance, with R and R^2 values of 0.97 and 0.95 (Table 1, Figures 8c, S6b and S7b). Thus, slide scar height increases with increasing down-slide scar distance and LPS depth (Figure 8c).

Slide scar widths vary from 840 m to 3000 m in the proximal areas, whereas the widths vary from 4300 m to 7500 m in the distal areas (Table 1 and Figure 8d). Additionally, the slide scars' base widths in the proximal areas vary from 380 m to 2000 m, whereas in the distal areas, they can reach up to 4000 m (Figure 8d). Regarding the correlations between the slide scars' widths and down-slide scar distance, Slide scar 1 has low values of R and R^2, whereas Slide scar 2

has high values of R and R^2 (Table 1, Figures S6c and S7c). The ratio of the top and base width for slide scar 1 is low (0.22), and that for slide scar 2 is relatively high (0.6) (Table 1). In addition, the general sinuosity of the slide scars in the proximal and distal areas is straight, with a sinuosity index value of 1.01 (Figure 8 and Figures S6c – S7c). The aspect ratios estimated for Slide scar 1 vary from 12.38 to 22.76, and the values estimated for Slide scar 2 are > 9.64 (Table 1). In addition, the CSA vary from 0.1 km^2 to 0.9 km^2 in proximal areas and from 0.6 km^2 to 2.5 km^2 in distal areas, yielding good to high R and R^2 values of > 0.8 (Figures 8e, S6d, and S7d). The slide scars in the study area have morphometric elements that show increasing values towards the distal parts of the slide scars.

5.3 Gullies

The four gullies identified in this work are located in the western part of the study area (Figure 4b). The gullies are orientated NW - SE, and the average preserved length of the gullies is approximately 1500 m (Figure 4b). The four gullies are V- and U-shaped (Figures 9 and 10a). The general sinuosity of the gullies in the study area is characterized as straight to low, with a minimum value of 1.00 and maximum value of 1.28 (Table 1).

5.3.1 Depositional elements of the filling deposits

The gullies in the study area are filled by Massive Low Amplitude Reflection Elements (Figures 2 and 9), which are characterized by massive, low to very low amplitude seismic reflections and parallel to subparallel reflections (Figures 2 and 9).

5.3.2 Gully architectural elements

The four elements of gully architecture observed in the study area are gully bases (including thalwegs), walls and flanks (Figures 2 and 9). The gully bases for the first type of gully are U-shaped and typified by dipping reflectors (< 20°). Continuous, medium to high seismic amplitude reflections dominate the U-shaped gully bases at the distal parts of the gully systems (Figure 9). V-shaped gully bases form another type and are typified by continuous, low to high seismic amplitude reflections that are relatively low dipping (< 20°) in the proximal domains (Figure 9). Gully walls are continuations of the gully bases and are characterized by low to high amplitude, long (200 - 500 m) dipping reflections (> 10°) that are seldom faulted (Figure 9). In the study area, two types of gully flanks have been observed and include flat and dipping flanks, with both types comprising parallel-subparallel, low to high seismic amplitude, continuous-discontinuous reflections (Figures 2 and 9).

5.3.3 Quantitative morphometric analysis of the gullies

In contrast to both the canyons and slide scars, the gullies in the study area can have both V-shaped and U-shaped morphologies (Figures 9 and 10a). The V-shaped gullies are associated with steep flank and gully walls, whereas the U-shaped gullies are associated with more than 100 m long-distance walls and flanks (Figure 9). In the proximal parts of the gullies, they vary in depth between 550 m and 700 m and have average gradients of 1.6°, whereas the distal gullies can reach depths up to 780 m with gradients of 0.4° (Figure 10b). The gradients of the gullies decrease down slope, giving high R and R^2 (average = 0.9) between gully depth and down-gully distance (Figure 10b and Figures S8a – S11a). A similar trend is observed for gully height and down-gully distance, with high values of R and R^2 for Gully 2 of 0.97 and 0.94, respectively, and 0.95 and 0.91 for Gully 4, respectively. The heights of the proximal gullies can range from 25 m to 70 m, reaching a maximum of 105 m in the distal parts (Figures 10c). In general, the width profiles of the gullies and gully bases show a parallel trend from the proximal to distal areas of the gully system, with an increasing trend to distal areas (Figure 10d, and Figures S8c – S11c). From the proximal to distal areas, the gully widths can vary from 250 m to 600 m, whereas gully base widths are in the range of 45 m to 250 m (Figure 10d). However, there is a poor correlation between gully width and down-gully distance for Gully 3, with R and R^2 values of < 0.4 (Figures 10d and S10c). Consequently, the aspect ratios of the gullies in the study area can reach a maximum of 11 in the proximal areas and 9.8 in the distal areas of the Loppa High (Table 1). In addition, the ratios of the tops and base gully widths show relatively low numbers of 0.28 and 0.31 (Table 1). The straight gullies (average values of 1.02) dominated the medial and distal areas of the gully system (Table 1 and Figure 10). On the contrary, three sinuosity anomalies are observed in the gully system of the study area: 1) the proximal part of gully 1, where the sinuosity index is 1.19 (Figures S8c), 2) the proximal part of gully 2, where the sinuosity index is 1.25 (Figures S9c) and 3) the medial part of gully 3, where the sinuosity index is 1.28 (Figure S10c). These anomalies are also represented as knickpoints in map view (Figure 10a). Additionally, in proximal areas, the CSA can vary from 0.008 km^2 to 0.03 km^2 and reach up to 0.06 km^2 in the distal areas (Figure 10e). There are good correlations between gully CSA and down-gully distance, with good and high R and R^2 values for Gully 2 and Gully 4, respectively (Figures S9d and S11d).

6.0 Discussion

6.1 Development of canyons and other sediment conduits

The development of the southern Loppa High sediment conduit systems can be divided into three different stages. The first stage occurred in the Late Jurassic-Cretaceous, when the currents at the base of canyon eroded the southern part of the Loppa High and transferred

sediments to the basin floor in the south (Faleide *et al.* 1993; Richardsen *et al.* 1993). The deposited sediments are interpreted as submarine fans as identified from present day seismic data (Figures 1b, 4c and 11a). During the Late Jurassic to Early Cretaceous, uplift and subsequent erosion of the Loppa High produced large amounts of sediments sourced from terrestrial areas in the north, which were transferred through the sediment conduits to the basin in the south (Figures 1c, 4 and 11a). In addition, during most of the Cretaceous, the Loppa High was an island produced by tectonic uplift, with deep canyons cutting into the Triassic sequence (Faleide *et al.* 1993; Richardsen *et al.* 1993). This hypothesis is further supported by the regional sea-level curve, which shows that the area witnessed a relative sea-level fall during the Late Jurassic to Early Cretaceous (Miller *et al.* 2005). In addition, the deep canyon in the study area has a height that ranges from 30 m to 417 m (Table 1, Figures 5 and 6c) and a canyon width from 237 m to 4409 m (Table 1, Figures 5 and 6d). The erosional events were responses to footwall uplift along the western boundary of the Loppa High and were possibly supported by lateral heat transfer from the rift basin in the south and west (Wood *et al.* 1989; Faleide *et al.* 1993). Furthermore, the upward-directed movement of the Loppa High is thus likely to have been converted into horizontal compressive stress along the flanks of the Loppa High. Stress generated by this mechanism would propagated perpendicularly in a N-S direction (Indrevær *et al.* 2016), possibly triggering slope failures at the flanks of the Loppa High. Evidence for slope failures during this event includes the initiation of the canyon escarpment on the edge of the Loppa High and two slide scars (Figures 5, 6a, 7, 8a, 11a and 11b).

By applying the sequence stratigraphic terminology of Posamentier & Vail (1988) to the Triassic and Jurassic sediments delivered to the basin in the south through the canyon systems, deposition during a relative sea-level fall implies these sediments are a “Lowstand System Tract” (Figure 11a). Consequently, lowstand fan deposition occurs when the rate of tectonic uplift exceeds the rate of eustatic rise at the physiographic shelf or slope break resulting in a relative decline in sea-level (Posamentier et al., 1991). This created subaerial exposure on the upper slope where the slope angle was steeper. In response, down cutting of streams commenced in association with the subaerial exposure of the shelf. The canyon system in the study area also shows different responses to slope angle; a sinuosity of 1.02 (straight) is dominant on the upper slope (proximal), a sinuosity of 1.06 (low sinuous) is dominant in the middle slope, and the straight canyon is dominant in the lower slope (distal) with an average sinuosity of 1.03 (Table 1, Figures 1b, 6 and S1c – S5c). Subsequently, the sediment load was directly delivered to the stream-mouth or near the shelf edge (Figures 11a and 11b). The total sediment load delivered to the shelf edge is further supplemented and enhanced with materials that have been excavated from the submarine canyon (Vail *et al.* 1977; Van Wagoner *et al.* 1988; Galloway 1989; Posamentier *et al.* 1991; Catuneanu 2006).

In addition, the HARE is located at the base of the canyon system and may correlate to the first stage of erosional phase and compaction. Given a throw of 2 km to 4 km on the western fault zone of the Loppa High, the amount of section removed in response to the Late Jurassic-Early Cretaceous uplift and erosion could, in fact, be in the range of 200-1200 m (Wood *et al.* 1989). In addition, longshore drift distributed the sediments parallel to the shoreline, leading to a seaward shift of the depocentre to the outer shelf or upper slope (Figures 11a and 11b) and contributing to an inherently unstable slope (Shepard 1963; Posamentier *et al.* 1991). This event might have contributed to the development of the canyons and slide scars in the study area. In addition, the gully system started after the initiation of slide scars, where the gully paths were not cut by the slide scars (Figure 8a). The longshore drift on the edge of the paleo Loppa high (Figures 1a and 11) likely contributed to the development of the gully system on the proximal and medial domains, which is indicated by the knickpoints and low sinuous pattern of gullies 1, 2 and 3 (Figures 10a and S8c – S10c).

The second stage occurred in the Paleogene, when regional subsidence centred along the North Atlantic rift basins produced pull-apart basins in the southwestern Barents Sea, and a relatively uniform and widespread sequence was deposited as sheets covering the entire western Barents Sea (Faleide *et al.* 1993; Faleide *et al.* 1996). This sequence infilled the southern Loppa High sediment conduits with MLARE and CRE (Figures 1b and 11c). Seismic sub-crop patterns, abnormally high interval velocities and well data indicate that more than 1000 m of Paleogene mudstones were deposited on the Loppa High, which were mostly eroded during the Cenozoic erosion (Wood *et al.* 1989; Faleide *et al.* 1993). In addition, Jobe *et al.* (2011) showed that the CREs are largely comprised of clay, indicating that they formed as drapes that blanket pre-existing topography and are not related to current activity. On the other hand, Posamentier & Kolla (2003) interpreted the MLARE as mud prone debris flow deposits. Lowstand wedges also occur during relative sea-level rise at the shelf edge and are characterized by the deposition of sediments within canyons, slopes, and basin floors (Posamentier & Vail 1985; Posamentier & Vail 1988; Posamentier *et al.* 1991). This significantly shifts the shoreline to the landward area, creating less of a denudation area (Figure 11c). Hence, fine-grained materials (as sheets covered) dominated the southern part of the Loppa High during this stage (Figure 11c). At that time, sediment loads delivered to the upper slope decreased as the canyons became depositional sites (Posamentier *et al.* 1991). Canyon walls, which were steepened during the interval of active canyon down-cutting (lowstand fan), became less steep through the processes of mass wasting, as the canyon walls tended to re-establish an equilibrium profile (Deptuck *et al.* 2007). During this interval, canyon widening occurs in conjunction with canyon filling (Figures 11b and 11c). This is indicated by the relatively low ratios between tops and base widths of the canyons (Table 1).

The last stage occurred in the Neogene-Quaternary, when uplift and glacial erosion occurred (Wood *et al.* 1989; Faleide *et al.* 1993; Miller *et al.* 2005), modulating the present southern Loppa High into a denudation area (Figure 11d). Seismic sub-crop patterns and well data indicate that Late Cenozoic erosion was approximately 500 m to 1000 m, whereas ice-related erosion during recent glaciation has enhanced the unconformity at the base of the Pliocene-Pleistocene (Wood *et al.* 1989; Faleide *et al.* 1993; Henriksen *et al.* 2011a).

6.2 Implications of the sediment conduits' morphologies for paleoenvironment reconstruction

In general, canyons dominate the study area (Figure 4), thus indicating that they are good sediment conduits (Shepard 1952; Kuenen 1953; Stow & Mayall 2000; Posamentier & Kolla 2003). Their morphologies and architectures also reveal spatial variations as erosion and back stepping of the shoreline occurred. This is evidenced by the general increases in the widths, heights, and cross-sectional areas in the distal canyon area (Figure 6). Those increasing parameters are possibly controlled by system distance, as more frequent and faster flows are mostly down-canyon, and because down-canyon movement is facilitated by gravity, net transport from these currents is largely seaward (Shepard & Marshall 1973; Shepard *et al.* 1974; Shepard 1981). In addition, Canyon 1 has the lowest height and length relative to the other canyons (Figure 6), a phenomenon that likely reflects the greater distance of Canyon 1 from the fluvial stream mouth of the denudation area (Table 1, Figures 11a, 11b, and 11c). Hence, only longshore-drift and tidal currents can distribute sediments to Canyon 1 and form unstable masses subject to slumping, sand flows, and turbidity currents (Shepard 1963; Shepard & Marshall 1973; Normark *et al.* 1993; Weaver *et al.* 2000; Flint & Hodgson 2005; Covault *et al.* 2011; Yu *et al.* 2013). Furthermore, these spatial variations are also indicated by the ratio of the top and base width of the canyon (Table 1). The lowest ratio found in canyon 1 shows less variation when compared to the highest top and base width canyon ratio for canyon 5 (Table 1). In addition, the U-shaped canyons are mostly located in the proximal part of the canyon system in the study area (Figures 5 and 6a). The proximal part of the canyon system is characterized by relatively shallow bathymetry with shallow marine influences (Figure 11), which affected morphology in the canyon system (Figure 6a). Furthermore, the U-shaped morphology and the lack of significant changes in the U-shaped morphometry indicate a long-lived process involving fine-grained sediment that can be carried over the shelf and upper slope into the canyon heads without significant erosion, e.g., Thornton (1984), Posamentier & Kolla (2003), Jobe *et al.* (2011), and Lonergan *et al.* (2013). Tributaries associated with Canyons 2, 4 and 5 are located in the upper and middle canyon areas (proximal and distal), with average sinuosities of 1.05 and 1.08 (low sinuosity), respectively (Figures S2, S4 and S5).

These indicated that they were created by long-lived processes with low flow energy (Shepard 1963; Shepard & Marshall 1973; Posamentier & Kolla 2003; Estrada *et al.* 2005; Wynn *et al.* 2007).

The U-shaped, wide, wavy to planar gliding plane slide scars in the study area are characteristic of slide scars reported elsewhere (Shanmugam *et al.* 1994; Bøe *et al.* 2000; Posamentier & Kolla 2003; Shanmugam 2006; Bull *et al.* 2009; Richardson *et al.* 2011; Omosanya & Alves 2013; Jo *et al.* 2015). The U-shape is narrower upslope and wider downslope (Figures 7 and 8a). These represent a slope failure at the shelf edge caused by tectonic activity and a high rate of sedimentation producing instability on the shelf edge (Bull *et al.* 2009; Omosanya & Alves 2013; Alves 2015; Omeru *et al.* 2016; Omosanya *et al.* 2016). The scours of the slide scars created irregularities in the paleo-seafloor, thus providing conduits for sediment gravity currents (O'Leary 1986; Shanmugam *et al.* 1994; Shanmugam 2006). The slide scars are therefore considered to mark the area of maximum strain endured by the paleo-seafloor (Omosanya & Alves 2013). Furthermore, the slide scar MLAREs with reflection-free seismic (sometimes continuous) and low seismic amplitudes located above the gliding planes of the slide scars probably indicate the deposition of suspended, very fine-grained sediments or mud prone debris-flow deposits that occurred in response to bottom-current activity and increased accommodation space (Figure 11c) (O'Leary 1995; Posamentier & Kolla 2003; Gamboa & Alves 2015).

All four gullies in the study area are relatively narrow and have uniform widths (Figure 10) in comparison with the canyons and slide scars (Figure 2). This is one of the common characteristics of gullies, according to Field *et al.* (1999), Stow & Mayall (2000), Jobe *et al.* (2011), and Lonergan *et al.* (2013). The lack of significant changes in gully morphometry in the study area indicates that they represent a long-lived process on the shelf edge to the slope (Lonergan *et al.* 2013). This is most evident by the regularity in the gully-widths (Table 1 and Figure 10d). In addition, localized mass wasting driven by tectonic activity and spring sapping processes such as groundwater discharge from a sedimented slope may result in a change in pore fluid pressure in a radius around each failure (Orange *et al.* 1994; Pratson *et al.* 2009; Shumaker *et al.* 2016). These processes might also contribute to the prolonged process of gully development. Since there is no significant change in gully widths from the proximal to distal parts, it implies that the gully gradients also represent the paleo-slope gradient. In addition, the height variations for gullies 1, 2 and 3 are likely related to stair steps in the gully bases (Figures 10a and 10c).

This study has revealed that the morphological parameters (depth, height, width and cross-sectional area) for the canyons, slide scars, and gullies often increase linearly with distance

along slope, irrespective of their shapes and associated depositional elements. Furthermore, morphometric analyses of sediment conduits play an important role in quantitative interpretations of related sedimentary processes and paleoenvironment.

6.3 Implications for hydrocarbon prospectivity in the study area

The interconnections between the sediment conduits and their products such as submarine fans have wider implications for hydrocarbon prospectivity in the study area and in many other frontier basins. In the study area, the canyons, slide scars, and gullies are mostly filled with a fine-grained material (MLARE) that could possibly act as a reservoir and source rocks (Doré 1995; Bouma 2000; Bouma 2001; Henriksen *et al.* 2011a; Henriksen *et al.* 2011b; Bohacs *et al.* 2013). The canyon HARE is interpreted as a result of the presence of coarse-grained sediments caused by erosive energetic flows (Jobe *et al.* 2011) that could form good hydrocarbon reservoirs, although it is volumetrically smaller than the other depositional elements in the study area (Figures 2, 5, and 6e). Furthermore, wellbores 7122/2-1 and 7122/4-1 penetrated fine-grained and coarse-grained submarine fans of the Early Cretaceous Knurr Formation and Late Jurassic Stø Formation and indicated that they have good porosity and permeability (Sattar *et al.* 2017). In Figures 1b, 4c and 11, we show classic examples of submarine fans that are fed by a canyon system and onlap to the slope. The scenario presents a situation where hydrocarbons can migrate up-dip from the fans on the hanging walls of the faults into the upper and younger stratigraphic sections in the footwalls, hence increasing the prospectivity of hydrocarbons in the study area. In contrast, a fault can act as a barrier to hydrocarbons, creating poor inter-reservoir connectivity, and an additional wellbore would be required to drain hydrocarbons from each compartment. The continuous CRE in the middle of the canyons and slide scars could provide potential seal rocks, whereas the bases of the sediment conduits' incisions can act as lateral traps (Figures 5 and 7). In terms of volume, significant amounts of reservoir volume are also achievable from canyons and slide scars, as indicated by the high values of cross-sectional area (Figures 6e and 8e). Additionally, up-slope stratigraphic pinch-outs (in the case of submarine fans) could also provide stratigraphic traps towards the slope and up-dip positions. Sediment transport models indicate that grain size and grain-size distribution as well as slope gradients are key variables dictating bypass-related pinch-out development, where systems with steep slopes and relatively fine maximum grain sizes likely offer the lowest risk for up-dip leakage (McCaffrey & Kneller 2001; Stevenson *et al.* 2015).

6.4 Morphometry comparison with other sediment conduit systems

The canyons in the study area have heights that range from 30 m – 400 m (Figure 12a) and are comparable to other canyons documented on the continental margins of Equatorial Guinea, West Africa (Jobe *et al.* 2011) and SE Brazil (Qin *et al.* 2016). The canyons in the system in the study area are 70 m – 4000 m wide (Figure 12b), whereas those reported in the works of Jobe *et al.* (2011) and Qin *et al.* (2016) are relatively less wide. These differences may be related to the flow properties, e.g., flow volume, grain size distribution and fluid saturation (sensu Shepard & Marshall 1973; May *et al.* 1983; Babonneau *et al.* 2004; Talling 2014; Qin *et al.* 2016). Furthermore, this work shows a slide scar system that is 80 m – 350 m in height (Figure 12c) and 800 – 7600 in wide (Figure 12d). This morphometry characteristic has also been documented from seismic data in the SW Great Bahama Bank (Jo *et al.* 2015) and SW Norway (Bøe *et al.* 2000). The down-slide scar distances in the study area are shorter than those of Jo *et al.* (2015), which is an indication that the slide-scar system here has recorded less slope failure than that on the SW Great Bahama Bank (Jo *et al.* 2015). Similarly, the down-gully distances for the gullies in the study area are possibly shorter due to their locations on a local bathymetric high, i.e., the Loppa High. A parameter that contrasts with those gully systems has been documented on other continental margins. The gullies in the study area have heights in the range of 20 m – 100 m (Figure 12e) and widths of 200 m – 600 m (Figure 12f). The gullies documented by Lonergan *et al.* (2013) on the passive margin of Gabon (West Africa) and by Gales *et al.* (2013) on the continental margin of Antarctica have similar heights and widths to those of the study area but differ in their down-gully distances.

7.0 Conclusions

The following are the main conclusions from this work.

1. Canyons, gullies, and slide scars are the predominant sediment conduits in the southern part of the Loppa High and formed during the Late Jurassic to Cretaceous.
2. The observed variations in canyon morphology appear to be related to the distance of the canyon system. The shapes and morphometries of the slide scars in the study area represent slope failures at the shelf edge caused by tectonic activity and high sedimentation rates, producing instabilities on the shelf edge. Furthermore, the lack of significant changes in gully morphometry in the study area indicate that they represent a long-lived process on the shelf edge to the slope, whereas the gully knickpoints are related to the longshore drift on the edge of the paleo Loppa high.
3. The morphometry analysis of the sediment conduits in the study area played an important role in the quantitative interpretation of the related sedimentary processes and paleoenvironment.

4. The seismic facies and morphology analyses of the sediment conduits in the study area showed that the canyons, slide scars and gullies have potential for hydrocarbon prospectivity.

References

ALVES, T.M. (2015) Submarine slide blocks and associated soft-sediment deformation in deep-water basins: A review. *Marine and Petroleum Geology*, 67: 262-285.

AMBLAS, D., CERAMICOLA, S., GERBER, T.P., CANALS, M., CHIOCCI, F.L., DOWDESWELL, J.A., HARRIS, P.T., HUVENNE, V.A., LAI, S.Y. & LASTRAS, G., 2018. Submarine Canyons and Gullies, Submarine Geomorphology. Springer, pp. 251-272.

BABONNEAU, N., SAVOYE, B., CREMER, M. & BEZ, M. (2004) Multiple terraces within the deep incised Zaire Valley (ZaïAngo Project): are they confined levees? *Geological Society, London, Special Publications*, 222(1): 91-114.

BOHACS, K.M., PASSEY, Q.R., RUDNICKI, M., ESCH, W.L. & LAZAR, O.R. (2013) The Spectrum of Fine-Grained Reservoirs from shale gas to shale oil/ tight liquids: Essential attributes, key controls, practical characterization. International Petroleum Technology Conference.

BOUMA, A. (2001) Geological Architecture and Reservoir Characteristics of Fine-Grained and Coarse-Grained Turbidite Systems. *Houston Geological Society Bulletin*, 43(9): 23-33.

BOUMA, A.H. (2000) Coarse-grained and fine-grained turbidite systems as end member models: applicability and dangers. *Marine and Petroleum Geology*, 17(2): 137-143.

BROTHERS, D.S., TEN BRINK, U.S., ANDREWS, B.D., CHAYTOR, J.D. & TWICHELL, D.C. (2013) Geomorphic process fingerprints in submarine canyons. *Marine Geology*, 337(Supplement C): 53-66.

BULL, S., CARTWRIGHT, J. & HUUSE, M. (2009) A review of kinematic indicators from mass-transport complexes using 3D seismic data. *Marine and Petroleum Geology*, 26(7): 1132-1151.

BØE, R., HOVLAND, M., INSTANES, A., RISE, L. & VASSHUS, S. (2000) Submarine slide scars and mass movements in Karmsundet and Skudenesfjorden, southwestern Norway: morphology and evolution. *Marine Geology*, 167(1): 147-165.

CATTERALL, V., REDFERN, J., GAWTHORPE, R., HANSEN, D. & THOMAS, M. (2010) Architectural style and quantification of a submarine channel–levee system located in a structurally complex area: offshore Nile Delta. *Journal of Sedimentary Research*, 80(11): 991-1017.

CATUNEANU, O. (2006) *Principles of sequence stratigraphy*. Elsevier.

CLARK, J.D. & PICKERING, K.T. (1996) Architectural elements and growth patterns of submarine channels: application to hydrocarbon exploration. *AAPG bulletin*, 80(2): 194-220.

COVAULT, J. (2011) Submarine fans and canyon-channel systems: a review of processes, products, and models. *Nature Education Knowledge*, 3(10): 4.

COVAULT, J.A. & GRAHAM, S.A. (2010) Submarine fans at all sea-level stands: Tectono-morphologic and climatic controls on terrigenous sediment delivery to the deep sea. *Geology*, 38(10): 939-942.

COVAULT, J.A., ROMANS, B.W., GRAHAM, S.A., FILDANI, A. & HILLEY, G.E. (2011) Terrestrial source to deep-sea sink sediment budgets at high and low sea levels: Insights from tectonically active Southern California. *Geology*, 39(7): 619-622.

DEPTUCK, M.E., PIPER, D.J.W., SAVOYE, B. & GERVAIS, A. (2008) Dimensions and architecture of late Pleistocene submarine lobes off the northern margin of East Corsica. *Sedimentology*, 55(4): 869-898.

DEPTUCK, M.E., SYLVESTER, Z., PIRMEZ, C. & O'BYRNE, C. (2007) Migration–aggradation history and 3-D seismic geomorphology of submarine channels in the Pleistocene Benin-major Canyon, western Niger Delta slope. *Marine and Petroleum Geology*, 24(6–9): 406-433.

DORÉ, A. (1995) Barents Sea geology, petroleum resources and commercial potential. *Arctic*: 207-221.

ESTRADA, F., ERCILLA, G. & ALONSO, B. (2005) Quantitative study of a Magdalena submarine channel (Caribbean Sea): implications for sedimentary dynamics. *Marine and Petroleum Geology*, 22(5): 623-635.

FALEIDE, J.I., SOLHEIM, A., FIEDLER, A., HJELSTUEN, B.O., ANDERSEN, E.S. & VANNESTE, K. (1996) Late Cenozoic evolution of the western Barents Sea-Svalbard continental margin. *Global and Planetary Change*, 12(1–4): 53-74.

FALEIDE, J.I., VÅGNES, E. & GUDLAUGSSON, S.T. (1993) Late Mesozoic-Cenozoic evolution of the south-western Barents Sea in a regional rift-shear tectonic setting. *Marine and Petroleum Geology*, 10(3): 186-214.

FARRE, J.A., MCGREGOR, B.A., RYAN, W.B. & ROBB, J.M. (1983) Breaching the shelfbreak: passage from youthful to mature phase in submarine canyon evolution. *SEPM Special Publication* 33: 25-39.

FIELD, M.E., GARDNER, J.V. & PRIOR, D.B. (1999) Geometry and significance of stacked gullies on the northern California slope. *Marine Geology*, 154(1–4): 271-286.

FILDANI, A. (2017) Submarine Canyons: A brief review looking forward. *Geology*, 45(4): 383-384.

FLINT, S.S. & HODGSON, D.M. (2005) Submarine slope systems: processes and products. *Geological Society, London, Special Publications*, 244(1): 1-6.

FRIEND, P.F., 1983. Towards the Field Classification of Alluvial Architecture or Sequence, Modern and Ancient Fluvial Systems. Blackwell Publishing Ltd., pp. 345-354.

GABRIELSEN, R.H., FAERSETH, R.B. & JENSEN, L.N. (1990) *Structural Elements of the Norwegian Continental Shelf. Pt. 1. The Barents Sea Region*. Norwegian Petroleum Directorate.

GALES, J.A., LARTER, R.D., MITCHELL, N.C. & DOWDESWELL, J.A. (2013) Geomorphic signature of Antarctic submarine gullies: Implications for continental slope processes. *Marine Geology*, 337: 112-124.

GALLOWAY, W.E. (1989) Genetic stratigraphic sequences in basin analysis I: architecture and genesis of flooding-surface bounded depositional units. *AAPG bulletin*, 73(2): 125-142.

GAMBOA, D. & ALVES, T.M. (2015) Spatial and dimensional relationships of submarine slope architectural elements: A seismic-scale analysis from the Espírito Santo Basin (SE Brazil). *Marine and Petroleum Geology*, 64: 43-57.

GAMBOA, D., ALVES, T.M. & CARTWRIGHT, J. (2012) A submarine channel confluence classification for topographically confined slopes. *Marine and Petroleum Geology*, 35(1): 176-189.

GOODWIN, R.H. & PRIOR, D.B. (1989) Geometry and depositional sequences of the Mississippi Canyon, Gulf of Mexico. *Journal of Sedimentary Research*, 59(2).

GRADSTEIN, F.M., ANTHONISSEN, E., BRUNSTAD, H., CHARNOCK, M., HAMMER, O., HELLEM, T. & LERVIK, K.S. (2010) Norwegian offshore stratigraphic lexicon (NORLEX). *Newsletters on Stratigraphy*, 44(1): 73-86.

HAFLIDASON, H., SEJRUP, H.P., NYGÅRD, A., MIENERT, J., BRYN, P., LIEN, R., FORSBERG, C.F., BERG, K. & MASSON, D. (2004) The Storegga Slide: architecture, geometry and slide development. *Marine Geology*, 213(1): 201-234.

HANSEN, L., JANOCKO, M., KANE, I. & KNELLER, B. (2017) Submarine channel evolution, terrace development, and preservation of intra-channel thin-bedded turbidites: Mahin and Avon channels, offshore Nigeria. *Marine Geology*, 383: 146-167.

HARRIS, P.T. & WHITEWAY, T. (2011) Global distribution of large submarine canyons: Geomorphic differences between active and passive continental margins. *Marine Geology*, 285(1–4): 69-86.

HENRIKSEN, E., BJØRNSETH, H., HALS, T., HEIDE, T., KIRYUKHINA, T., KLØVJAN, O., LARSSEN, G., RYSETH, A., RØNNING, K. & SOLLID, K. (2011a) Uplift and erosion of the greater Barents Sea: impact on prospectivity and petroleum systems. *Geological Society, London, Memoirs*, 35(1): 271-281.

HENRIKSEN, E., RYSETH, A., LARSSEN, G., HEIDE, T., RØNNING, K., SOLLID, K. & STOUPAKOVA, A. (2011b) Tectonostratigraphy of the greater Barents Sea: implications for petroleum systems. *Geological Society, London, Memoirs*, 35(1): 163-195.

INDREVÆR, K., GABRIELSEN, R.H. & FALEIDE, J.I. (2016) Early Cretaceous synrift uplift and tectonic inversion in the Loppa High area, southwestern Barents Sea, Norwegian shelf. *Journal of the Geological Society*.

JAMES, G., WITTEN, D., HASTIE, T. & TIBSHIRANI, R. (2013) *An introduction to statistical learning*, 112. Springer.

JO, A., EBERLI, G.P. & GRASMUECK, M. (2015) Margin collapse and slope failure along southwestern Great Bahama Bank. *Sedimentary Geology*, 317: 43-52.

JOBE, Z.R., LOWE, D.R. & UCHYTIL, S.J. (2011) Two fundamentally different types of submarine canyons along the continental margin of Equatorial Guinea. *Marine and Petroleum Geology*, 28(3): 843-860.

KLAUS, A. & TAYLOR, B. (1991) Submarine canyon development in the Izu-Bonin forearc: A SeaMARC II and seismic survey of Aoga Shima Canyon. *Marine Geophysical Researches*, 13(2): 131-152.

KOLLA, V. (2007) A review of sinuous channel avulsion patterns in some major deep-sea fans and factors controlling them. *Marine and Petroleum Geology*, 24(6): 450-469.

KUENEN, P.H. (1953) ORIGIN AND CLASSIFICATION OF SUBMARINE CANYONS. *Geological Society of America Bulletin*, 64(11): 1295-1314.

LEE, S.H. & STOW, D.A.V. (2007) Laterally contiguous, concave-up basal shear surfaces of submarine landslide deposits (Miocene), southern Cyprus: differential movement of sub-blocks within a single submarine landslide lobe. *Geosciences Journal*, 11(4): 315-321.

LONERGAN, L., JAMIN, N.H., JACKSON, C.A.L. & JOHNSON, H.D. (2013) U-shaped slope gully systems and sediment waves on the passive margin of Gabon (West Africa). *Marine Geology*, 337: 80-97.

MARÍN, D., ESCALONA, A., ŚLIWIŃSKA, K.K., NØHR-HANSEN, H. & MORDASOVA, A. (2016) Sequence stratigraphy and lateral variability of Lower Cretaceous clinoforms in the southwestern Barents Sea. *AAPG Bulletin*(20,161,221).

MATTOS, N.H., ALVES, T.M. & OMOSANYA, K.O. (2016) Crestal fault geometries reveal late halokinesis and collapse of the Samson Dome, Northern Norway: Implications for petroleum systems in the Barents Sea. *Tectonophysics*, 690, Part A: 76-96.

MAY, J.A., WARME, J.E. & SLATER, R.A. (1983) Role of submarine canyons on shelfbreak erosion and sedimentation: modern and ancient examples. *SEPM Special Publication*, 33: 315-332.

MAYALL, M., JONES, E. & CASEY, M. (2006) Turbidite channel reservoirs—Key elements in facies prediction and effective development. *Marine and Petroleum Geology*, 23(8): 821-841.

MCCAFFREY, W. & KNELLER, B. (2001) Process controls on the development of stratigraphic trap potential on the margins of confined turbidite systems and aids to reservoir evaluation. *AAPG bulletin*, 85(6): 971-988.

MIALL, A.D. (1989) Architectural elements and bounding surfaces in channelized clastic deposits: Notes on comparisons between fluvial and turbidite systems. *Sedimentary facies in the active plate margin: Tokyo, Terra Scientific Publishing Company*: 3-15.

MILLER, K.G., KOMINZ, M.A., BROWNING, J.V., WRIGHT, J.D., MOUNTAIN, G.S., KATZ, M.E., SUGARMAN, P.J., CRAMER, B.S., CHRISTIE-BLICK, N. & PEKAR, S.F. (2005) The Phanerozoic record of global sea-level change. *science*, 310(5752): 1293-1298.

MOUNTJOY, J.J., BARNES, P.M. & PETTINGA, J.R. (2009) Morphostructure and evolution of submarine canyons across an active margin: Cook Strait sector of the Hikurangi Margin, New Zealand. *Marine Geology*, 260(1): 45-68.

MUTTI, E. & NORMARK, W.R., 1987. Comparing Examples of Modern and Ancient Turbidite Systems: Problems and Concepts. In: J.K. Leggett and G.G. Zuffa (Editors), Marine Clastic Sedimentology: Concepts and Case Studies. Springer Netherlands, Dordrecht, pp. 1-38.

MUTTI, E. & NORMARK, W.R., 1991. An Integrated Approach to the Study of Turbidite Systems. In: P. Weimer and M.H. Link (Editors), Seismic Facies and Sedimentary Processes of Submarine Fans and Turbidite Systems. Springer New York, New York, NY, pp. 75-106.

NORMARK, W.R. & CARLSON, P.R. (2003) Giant submarine canyons: Is size any clue to their importance in the rock record? *Geological Society of America Special Papers*, 370: 175-190.

NORMARK, W.R., POSAMENTIER, H. & MUTTI, E. (1993) Turbidite systems: State of the art and future directions. *Reviews of Geophysics*, 31(2): 91-116.

O'LEARY, D.W. (1986) The Munson-Nygren slide: A major lower-slope slide off Georges Bank. *Marine Geology*, 72(1): 101-114.

O'LEARY, D.W., 1995. Canyon-filling debrite indicates that canyon erosion and large-scale mass movement off Georges Bank, USA, are unrelated processes. In: K.T. Pickering, R.N. Hiscott, N.H. Kenyon, F. Ricci Lucchi and R.D.A. Smith (Editors), Atlas of Deep Water Environments: Architectural style in turbidite systems. Springer Netherlands, Dordrecht, pp. 23-25.

OBELCZ, J., BROTHERS, D., CHAYTOR, J., BRINK, U.T., ROSS, S.W. & BROOKE, S. (2014) Geomorphic characterization of four shelf-sourced submarine canyons along the U.S. Mid-Atlantic continental margin. *Deep Sea Research Part II: Topical Studies in Oceanography*, 104(Supplement C): 106-119.

OMERU, T., CARTWRIGHT, J.A. & BULL, S., 2016. Kinematics of Submarine Slope Failures in the Deepwater Taranaki Basin, New Zealand. In: G. Lamarche, J. Mountjoy, S. Bull, T. Hubble, S. Krastel, E. Lane, A. Micallef, L. Moscardelli, C. Mueller, I. Pecher and S. Woelz (Editors), Submarine Mass Movements and their Consequences: 7th International Symposium. Springer International Publishing, Cham, pp. 61-70.

OMOSANYA, K.D.O. & ALVES, T.M. (2013) Ramps and flats of mass-transport deposits (MTDs) as markers of seafloor strain on the flanks of rising diapirs (Espírito Santo Basin, SE Brazil). *Marine Geology*, 340: 82-97.

OMOSANYA, K.O., HARISHIDAYAT, D., MARHENI, L., JOHANSEN, S.E., FELIX, M. & ABRAHAMSON, P. (2016) Recurrent mass-wasting in the Sørvestsnaget Basin Southwestern Barents Sea: A test of multiple hypotheses. *Marine Geology*, 376: 175-193.

ORANGE, D.L., ANDERSON, R.S. & BREEN, N.A. (1994) Regular canyon spacing in the submarine environment: the link between hydrology and geomorphology. *GSA Today*, 4(2): 35-39.

ORTIZ-KARPF, A., HODGSON, D.M., JACKSON, C.A.-L. & MCCAFFREY, W.D. (2017) Influence of Seabed Morphology and Substrate Composition On Mass-Transport Flow Processes and Pathways: Insights From the Magdalena Fan, Offshore Colombia. *Journal of Sedimentary Research*, 87(3): 189-209.

PAQUET, F., PROUST, J.-N., BARNES, P.M. & PETTINGA, J.R. (2009) Inner-Forearc Sequence Architecture in Response to Climatic and Tectonic Forcing Since 150 ka: Hawke's Bay, New Zealand. *Journal of Sedimentary Research*, 79(3): 97-124.

POSAMENTIER, H. & VAIL, P. (1985) Eustatic Control on Depositional Stratal Patterns, Soc. Econ. Pal. Min. Research Conference, Sea-level changes: An Integrated Approach.

POSAMENTIER, H. & VAIL, P. (1988) Eustatic controls on clastic deposition II—sequence and systems tract models. *SEPM Special Publication*, 42(Sea level changes - An integrated approach).

POSAMENTIER, H. & WALKER, R.G. (2006) Deep-water turbidites and submarine fans. *Facies models revisited, vol.84, SEPM Special Publication*: 397-520.
POSAMENTIER, H.W., ERSKINE, R.D. & MITCHUM, R.M., 1991. Models for Submarine-Fan Deposition within a Sequence-Stratigraphic Framework. In: P. Weimer and M.H. Link (Editors), Seismic Facies and Sedimentary Processes of Submarine Fans and Turbidite Systems. Springer New York, New York, NY, pp. 127-136.
POSAMENTIER, H.W. & KOLLA, V. (2003) Seismic Geomorphology and Stratigraphy of Depositional Elements in Deep-Water Settings. *Journal of Sedimentary Research*, 73(3): 367-388.
PRATSON, L.F., NITTROUER, C.A., WIBERG, P.L., STECKLER, M.S., SWENSON, J.B., CACCHIONE, D.A., KARSON, J.A., MURRAY, A.B., WOLINSKY, M.A., GERBER, T.P., MULLENBACH, B.L., SPINELLI, G.A., FULTHORPE, C.S., O'GRADY, D.B., PARKER, G., DRISCOLL, N.W., BURGER, R.L., PAOLA, C., ORANGE, D.L., FIELD, M.E., FRIEDRICHS, C.T. & FEDELE, J.J., 2009. Seascape Evolution on Clastic Continental Shelves and Slopes, Continental Margin Sedimentation. Blackwell Publishing Ltd., pp. 339-380.
PRÉLAT, A., PANKHANIA, S.S., JACKSON, C.A.L. & HODGSON, D.M. (2015) Slope gradient and lithology as controls on the initiation of submarine slope gullies; Insights from the North Carnarvon Basin, Offshore NW Australia. *Sedimentary Geology*, 329: 12-17.
QIN, Y., ALVES, T.M., CONSTANTINE, J. & GAMBOA, D. (2016) Quantitative seismic geomorphology of a submarine channel system in SE Brazil (Espírito Santo Basin): Scale comparison with other submarine channel systems. *Marine and Petroleum Geology*, 78: 455-473.
REIMCHEN, A.P., HUBBARD, S.M., STRIGHT, L. & ROMANS, B.W. (2016) Using sea-floor morphometrics to constrain stratigraphic models of sinuous submarine channel systems. *Marine and Petroleum Geology*, 77(Supplement C): 92-115.
RICHARDSEN, G., VORREN, T.O. & TØRUDBAKKEN, B.O. (1993) Post-Early Cretaceous uplift and erosion in the southern Barents Sea: a discussion based on analysis of seismic interval velocities. *Norsk Geologisk Tidsskrift*, 73(1): 3-20.
RICHARDSON, S.E.J., DAVIES, R.J., ALLEN, M.B. & GRANT, S.F. (2011) Structure and evolution of mass transport deposits in the South Caspian Basin, Azerbaijan. *Basin Research*, 23(6): 702-719.
ROEP, T.B. & FORTUIN, A.R. (1996) A submarine slide scar and channel filled with slide blocks and megarippled Globigerina sands of possible contourite origin from the Pliocene of Sumba, Indonesia. *Sedimentary Geology*, 103(1): 145-160.
SATTAR, N., JUHLIN, C., KOYI, H. & AHMAD, N. (2017) Seismic stratigraphy and hydrocarbon prospectivity of the Lower Cretaceous Knurr Sandstone lobes along the southern margin of Loppa High, Hammerfest Basin, Barents Sea. *Marine and Petroleum Geology*, 85: 54-69.
SAYAGO-GIL, M., PÉREZ-GARCÍA, C., VÁZQUEZ, J., HERNÁNDEZ-MOLINA, F., FERNÁNDEZ-SALAS, L., ALVEIRINHO-DIAS, J., DÍAZ DEL RÍO, V. & SOMOZA, L. (2008) Slides on the flanks of submarine canyons in the upper slope of the Algarve. *Thalassas*, 24(1): 65-72.
SHANMUGAM, G. (2006) *Deep-water processes and facies models: Implications for sandstone petroleum reservoirs*, 5. Elsevier.
SHANMUGAM, G., LEHTONEN, L.R., STRAUME, T., SYVERTSEN, S.E., HODGKINSON, R.J. & SKIBELI, M. (1994) Slump and debris-flow dominated upper slope facies in the Cretaceous of the Norwegian and northern North Seas (61-67 N): Implications for sand distribution. *AAPG bulletin*, 78(6): 910-937.
SHEPARD, F.P. (1952) Composite Origin of Submarine Canyons. *The Journal of Geology*, 60(1): 84-96.
SHEPARD, F.P. (1963) Importance of submarine valleys in funneling sediments to the deep sea. *Progress in Oceanography*, 3: 321-332.
SHEPARD, F.P. (1965) Types of submarine valleys. *AAPG Bulletin*, 49(3): 304-310.

SHEPARD, F.P. (1972) Submarine canyons. *Earth-Science Reviews*, 8(1): 1-12.
SHEPARD, F.P. (1981) Submarine canyons: multiple causes and long-time persistence. *AAPG Bulletin*, 65(6): 1062-1077.
SHEPARD, F.P. & MARSHALL, N.F. (1973) Currents along floors of submarine canyons. *AAPG Bulletin*, 57(2): 244-264.
SHEPARD, F.P., MARSHALL, N.F. & MCLOUGHLIN, P.A. (1974) Currents in submarine canyons. *Deep Sea Research and Oceanographic Abstracts*, 21(9): 691-706.
SHUMAKER, L.E., JOBE, Z.R. & GRAHAM, S.A. (2016) Evolution of submarine gullies on a prograding slope: Insights from 3D seismic reflection data. *Marine Geology*.
STEVENSON, C.J., JACKSON, C.A.-L., HODGSON, D.M., HUBBARD, S.M. & EGGENHUISEN, J.T. (2015) Deep-water sediment bypass. *Journal of Sedimentary Research*, 85(9): 1058-1081.
STOW, D.A.V. & MAYALL, M. (2000) Deep-water sedimentary systems: New models for the 21st century. *Marine and Petroleum Geology*, 17(2): 125-135.
STOW, D.A.V., READING, H.G. & COLLINSON, J.D. (1996) Deep clastic seas. In: Reading, H.G. (Ed.), Sedimentary Environments and Facies. *Blackwell Scientific Publications, Oxford*, Third ed.: 399-444.
TALLING, P.J. (2014) On the triggers, resulting flow types and frequencies of subaqueous sediment density flows in different settings. *Marine Geology*, 352: 155-182.
THORNTON, S. (1984) Hemipelagites and associated facies of slopes and Slope Basins. *Geological Society of London, Special Publications*, 15: 377e394.
TUBAU, X., LASTRAS, G., CANALS, M., MICALLEF, A. & AMBLAS, D. (2013) Significance of the fine drainage pattern for submarine canyon evolution: The Foix Canyon System, Northwestern Mediterranean Sea. *Geomorphology*, 184(Supplement C): 20-37.
TUBAU, X., PAULL, C.K., LASTRAS, G., CARESS, D.W., CANALS, M., LUNDSTEN, E., ANDERSON, K., GWIAZDA, R. & AMBLAS, D. (2015) Submarine canyons of Santa Monica Bay, Southern California: Variability in morphology and sedimentary processes. *Marine Geology*, 365(Supplement C): 61-79.
VAIL, P.R., MITCHUM JR, R. & THOMPSON III, S. (1977) Seismic stratigraphy and global changes of sea level: Part 3. Relative changes of sea level from Coastal Onlap: section 2. Application of seismic reflection Configuration to Stratigrapic Interpretation.
VAN WAGONER, J., POSAMENTIER, H., MITCHUM, R., VAIL, P., SARG, J., LOUTIT, T. & HARDENBOL, J. (1988) An overview of the fundamentals of sequence stratigraphy and key definitions. *SEPM Society for Sedimentary Geology*, Special Publication No.42.
VÖLKER, D., GEERSEN, J., BEHRMANN, J.H. & WEINREBE, W.R., 2012. Submarine Mass Wasting Off Southern Central Chile: Distribution and Possible Mechanisms of Slope Failure at an Active Continental Margin. In: Y. Yamada, K. Kawamura, K. Ikehara, Y. Ogawa, R. Urgeles, D. Mosher, J. Chaytor and M. Strasser (Editors), Submarine Mass Movements and Their Consequences: 5th International Symposium. Springer Netherlands, Dordrecht, pp. 379-389.
WEAVER, P.P.E., WYNN, R.B., KENYON, N.H. & EVANS, J. (2000) Continental margin sedimentation, with special reference to the north-east Atlantic margin. *Sedimentology*, 47: 239-256.
WOOD, R., EDRICH, S. & HUTCHISON, I. (1989) Influence of North Atlantic Tectonics on the Large-Scale Uplift of the Stappen High and Loppa High, Western Barents Shelf: Chapter 36: North Sea and Barents Shelf.
WORSLEY, D. (2008) The post-Caledonian development of Svalbard and the western Barents Sea. *Polar Research*, 27(3): 298-317.
WYNN, R.B., CRONIN, B.T. & PEAKALL, J. (2007) Sinuous deep-water channels: Genesis, geometry and architecture. *Marine and Petroleum Geology*, 24(6): 341-387.
YU, G.-A., LIU, L., LI, Z., LI, Y., HUANG, H., BRIERLEY, G., BLUE, B., WANG, Z. & PAN, B. (2013) Fluvial diversity in relation to valley setting in the source region of the Yangtze and Yellow Rivers. *Journal of Geographical Sciences*, 23(5): 817-832.

ZIEBA, K.J., OMOSANYA, K.O. & KNIES, J. (2017) A flexural isostasy model for the Pleistocene evolution of the Barents Sea bathymetry. *NORWEGIAN JOURNAL OF GEOLOGY*, 97(1).

Table 1. Summary of morphometry data for canyons, gullies and slide scars.

	Depth (m)			Height (m)			Width (m)			Width Average (m)			Gradient (Deg)		
	Maximum	Minimum	Average	Maximum	Minimum	Average	Maximum	Minimum	Average	Top	Base	Ratio	Maximum	Minimum	Average
Canyon															
1	847	630	736	265	101	158	1631	393	992	992	157	0.16	3.01	0.18	0.72
2	1256	510	800	409	30	194	2850	240	1297	1479	304	0.21	4.96	0.06	0.54
3	1023	616	805	392	145	264	2405	579	1465	1465	240	0.16	3.88	0.12	0.63
4	1000	504	701	378	73	202	3730	237	1463	1653	402	0.24	3.10	0.04	0.29
5	1094	535	730	417	78	199	4409	537	1656	1989	409	0.21	5.91	0.03	0.23
Gully															
1	763	629	689	76	53	70	477	362	440	440	124	0.28	2.97	0.65	1.48
2	779	616	698	98	35	66	584	238	349	349	108	0.31	2.70	0.44	1.17
3	777	562	630	43	26	35	396	312	352	352	110	0.31	2.45	0.21	0.70
4	785	675	740	104	53	80	592	317	512	512	142	0.28	3.13	0.33	1.03
Slide Scar															
1	960	696	815	343	223	290	7600	3131	4663	4663	1032	0.22	2.63	0.24	0.78
2	900	650	772	213	88	152	5109	849	3146	3146	1888	0.6	2.38	0.24	0.77

	Sinuosity			Aspect Ratio (width/height)			Width vs Dist		Height vs Dist	
	Maximum	Minimum	Average	Maximum	Minimum	Average	R^2	R	R^2	R
Canyon										
1	1.19	1.00	1.03	10.44	2.72	6.46	0.44	0.66	0.41	0.64
2	1.30	1.00	1.04	10.33	3.87	6.81	0.64	0.80	0.83	0.91
3	1.32	1.00	1.02	6.90	2.60	5.41	0.27	0.52	0.43	0.66
4	1.58	1.00	1.07	13.91	2.72	6.92	0.63	0.79	0.66	0.81
5	1.40	1.00	1.09	16.32	4.57	8.05	0.41	0.64	0.54	0.73
Gully										
1	1.13	1.00	1.02	6.83	6.08	6.29	0.68	0.82	0.61	0.78
2	1.25	1.00	1.05	6.85	4.10	5.38	0.80	0.89	0.94	0.97
3	1.28	1.00	1.02	13.14	8.44	10.13	0.16	0.40	0.42	0.65
4	1.04	1.00	1.00	8	5.68	6.52	0.78	0.88	0.91	0.95
Slide Scar										
1	1.04	1.00	1.01	22.76	12.38	15.62	0.79	0.88	0.95	0.97
2	1.05	1.00	1.00	25.11	9.64	19.37	0.95	0.97	0.96	0.98

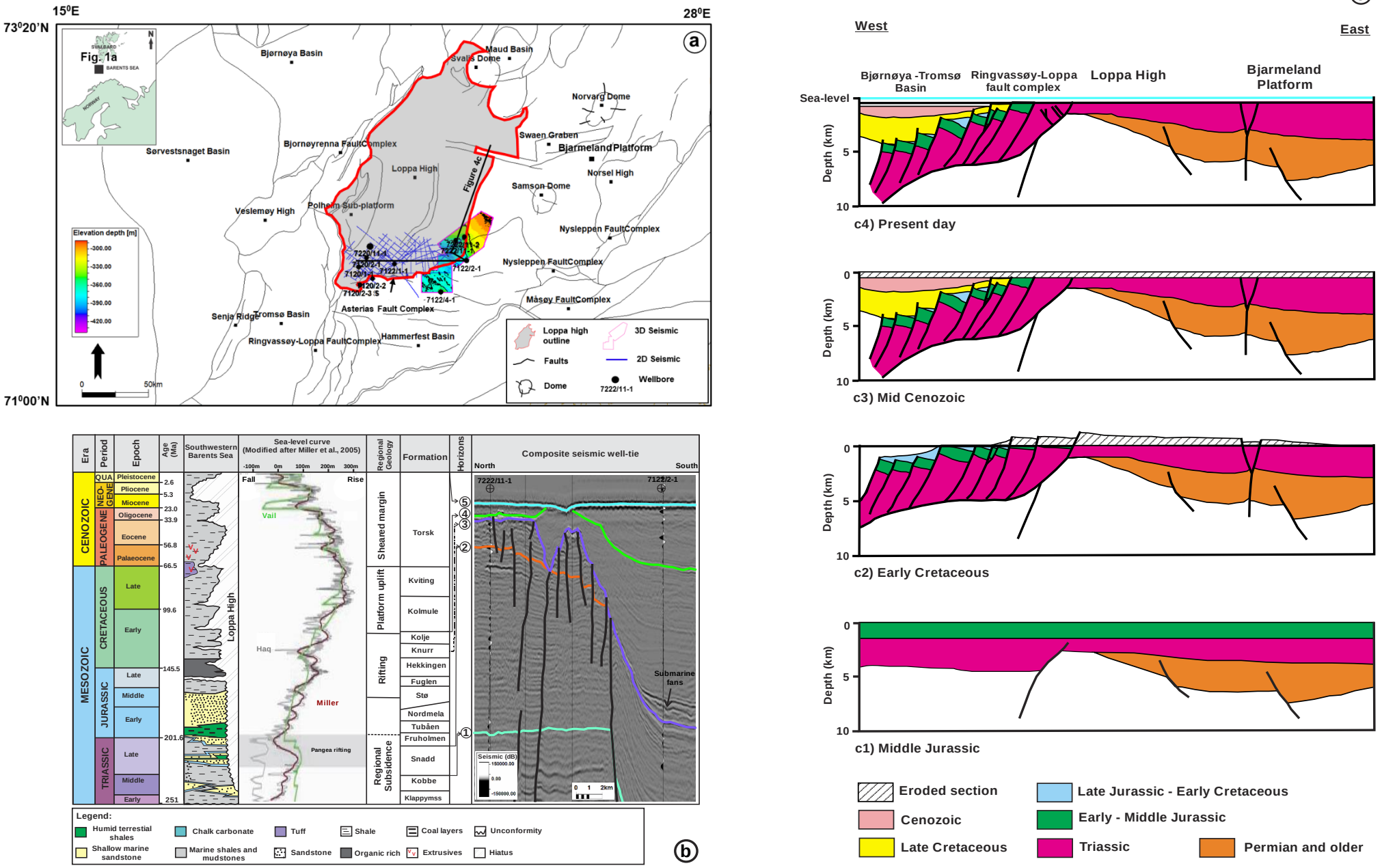

Figure 1. (a) Location map of the study area in the southern part of Loppa High with a seabed map from the 3-D seismic data. (b) Stratigraphic column of the SW Barents Sea area (Gradstein *et al. 2010*) with regional sea-level curve (Miller *et al*. 2005) and seismic well-tie in the study area. (c) Tectonic evolution of the Loppa High (modified after Wood *et al*. 1989).

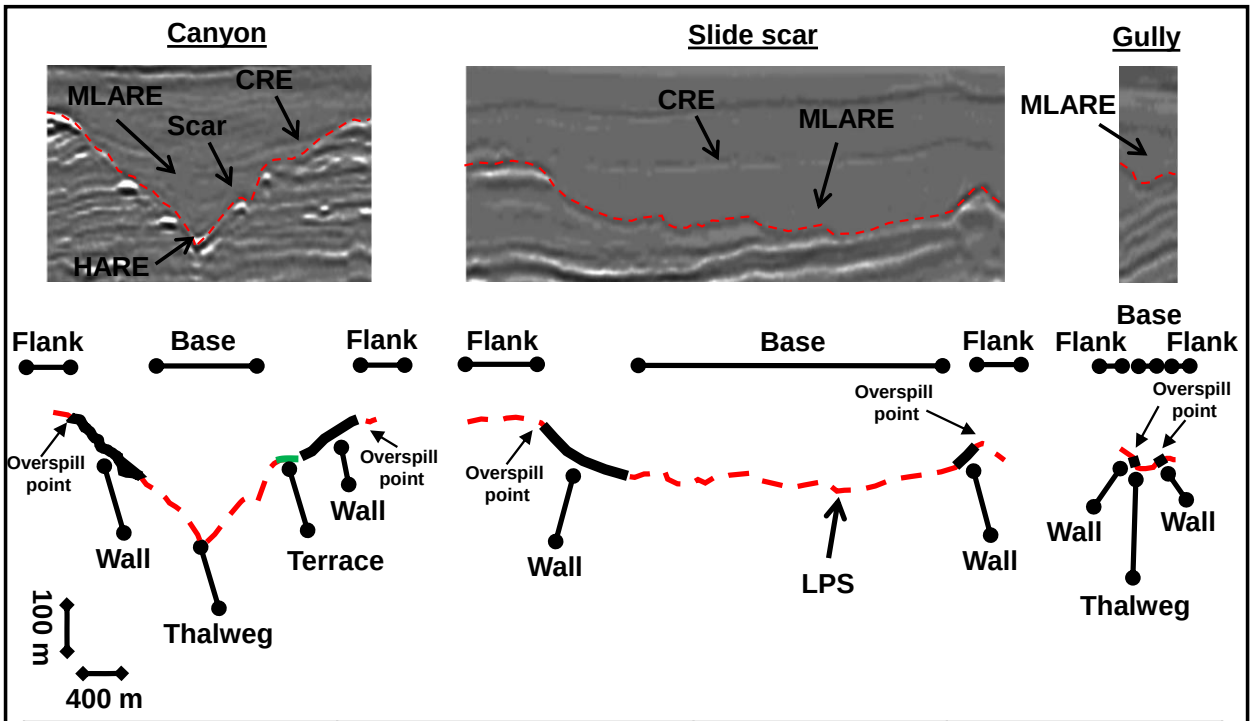

	Canyon	Slide scar	Gully
Depositional elements of filling deposit	Conformable Reflection Elements (CRE), Massive Low Amplitude Reflection Elements (MLARE), High Amplitude Reflection Elements (HARE) and Scar	CRE and MLARE	MLARE
Architectural elements of erosional surface	Base, thalweg, terrace, wall and flank	Base, the Lowest Point of Slide scar (LPS), wall and flank	Base, thalweg, wall and flank
Type of deposits	Sediment gravity flows with sand prone erosion during canyon initiation. Interbedded sandstone and shale (CRE; Jobe *et al*. 2011)	Slope failure filled by continous (CRE; Jobe *et al*. 2011) and massive (MLARE; Posamentier & Kolla 2003) fine grained material interpreted as debrite (O'leary 1995; Gamboa & Alves 2015)	Sediment gravity flows during gully initiation and fault influence, filled by relatively fine-grained material (MLARE; Posamentier & Kolla 2003)

Figure 2. Summary of different seismic facies analysed in this work. The red dash-line is the base of incision.

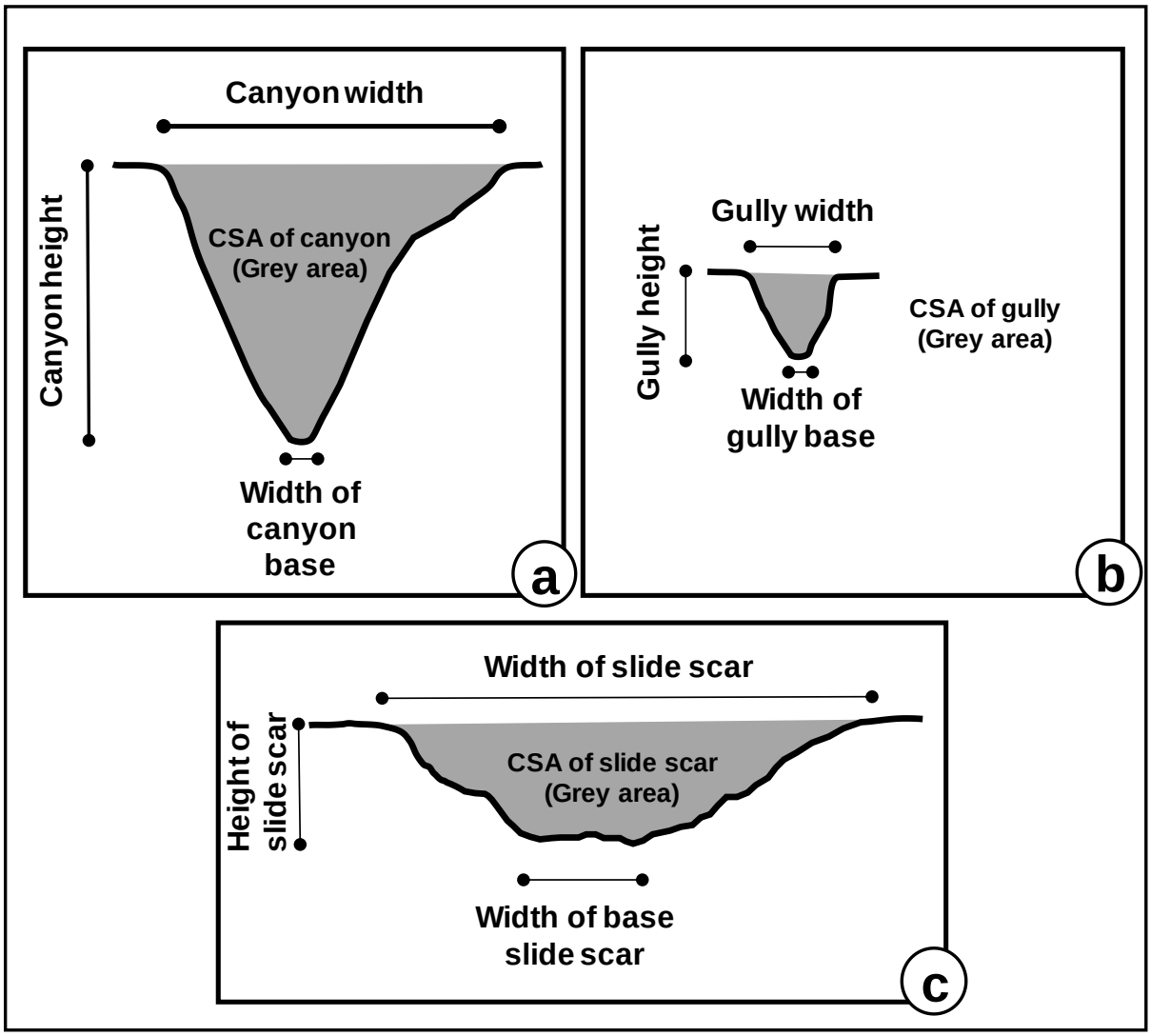

Figure 3. Morphometric elements of sediment conduits analysed in this study. *CSA denotes Cross Sectional Area.*

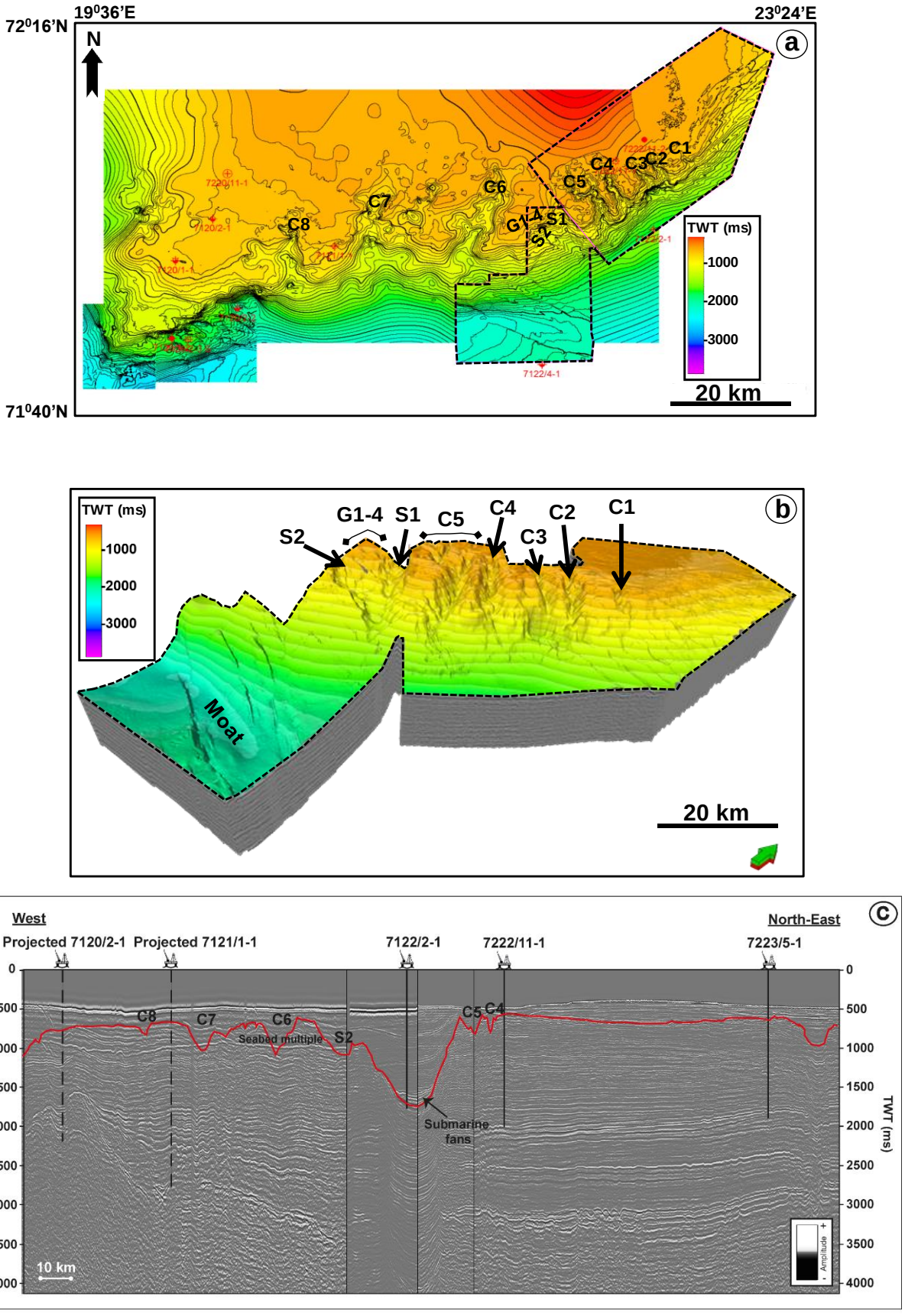

Figure 4. (a) Surface map of base sediment conduit system (Horizon 3) in the southern part of the Loppa High. Pink and black-dashed rectangle outline the location of the 3-D seismic data used in this study. (b) 3D surface of base sediment conduit system (Horizon 3) in the SE Loppa High derived from the inset in (a). (c) Regional seismic line showing a section that perpendicular to the sediment conduit system in the study area. Note that red line is an erosional surface. See figure 1a for line location. *C denotes Canyon, S denotes Slide scar, and G denotes Gully.*

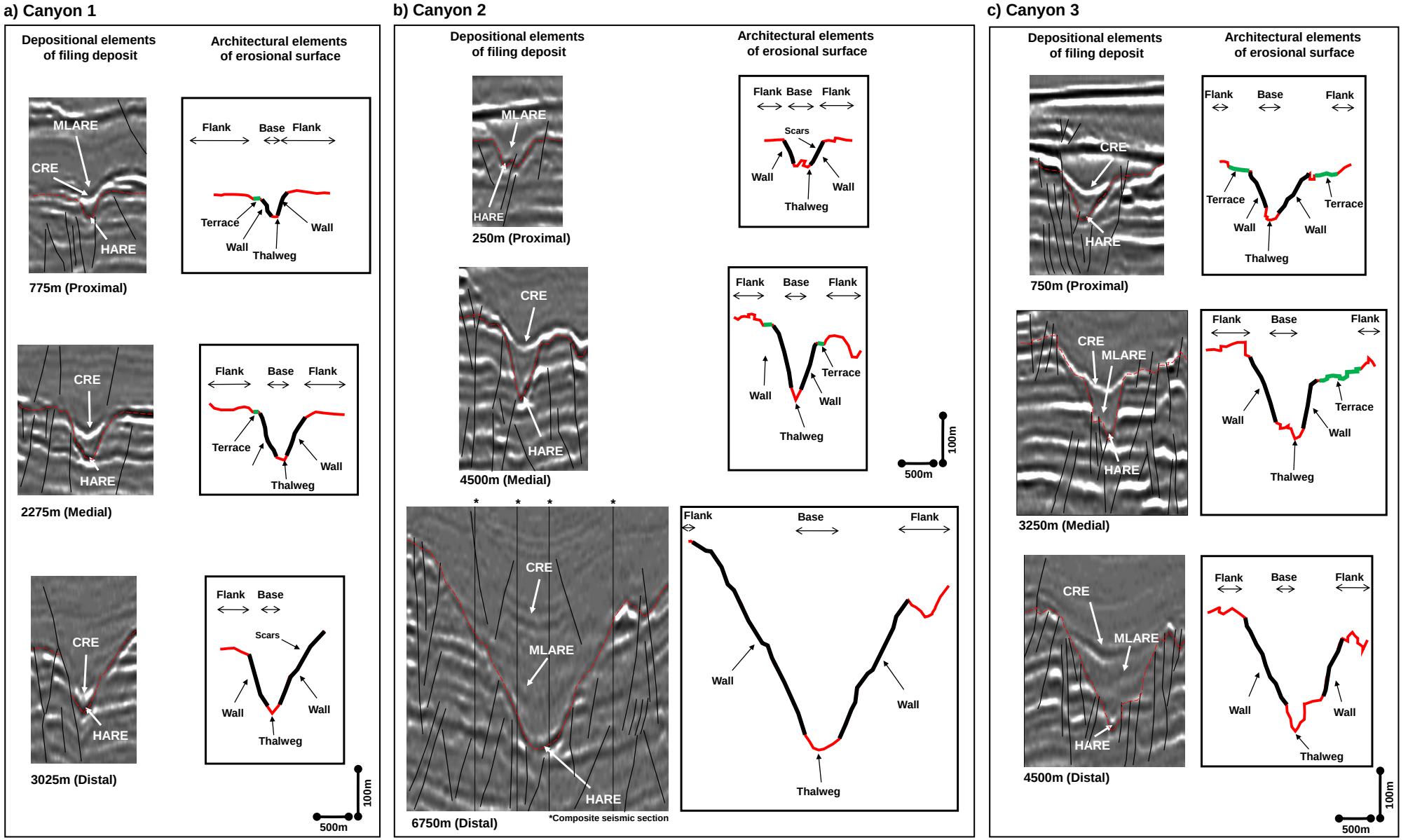

Figure 5. (Continued).

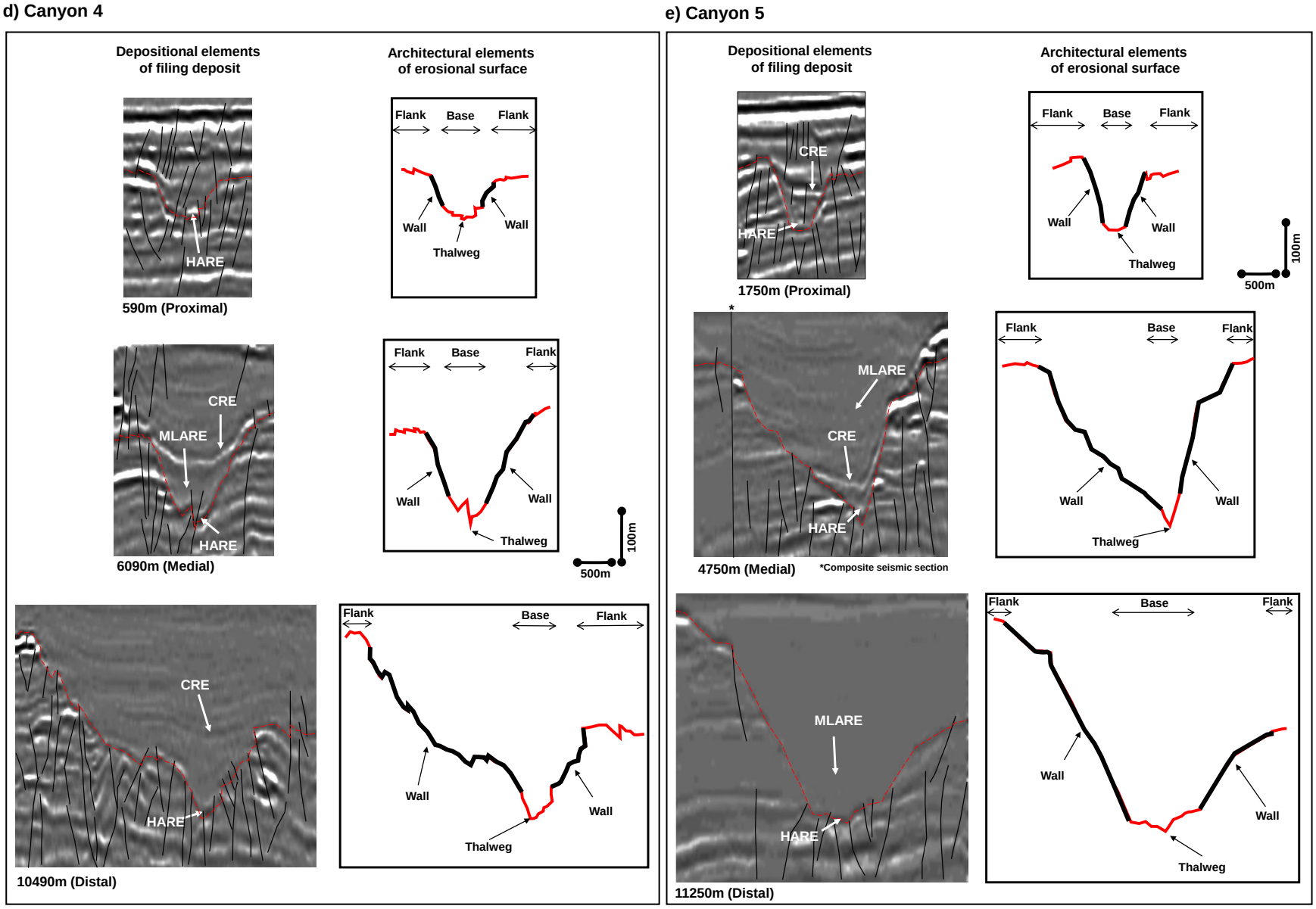

Figure 5. Seismic facies analysis of canyons in the study area, representing the proximal – distal system. See Figure 6a for section location.

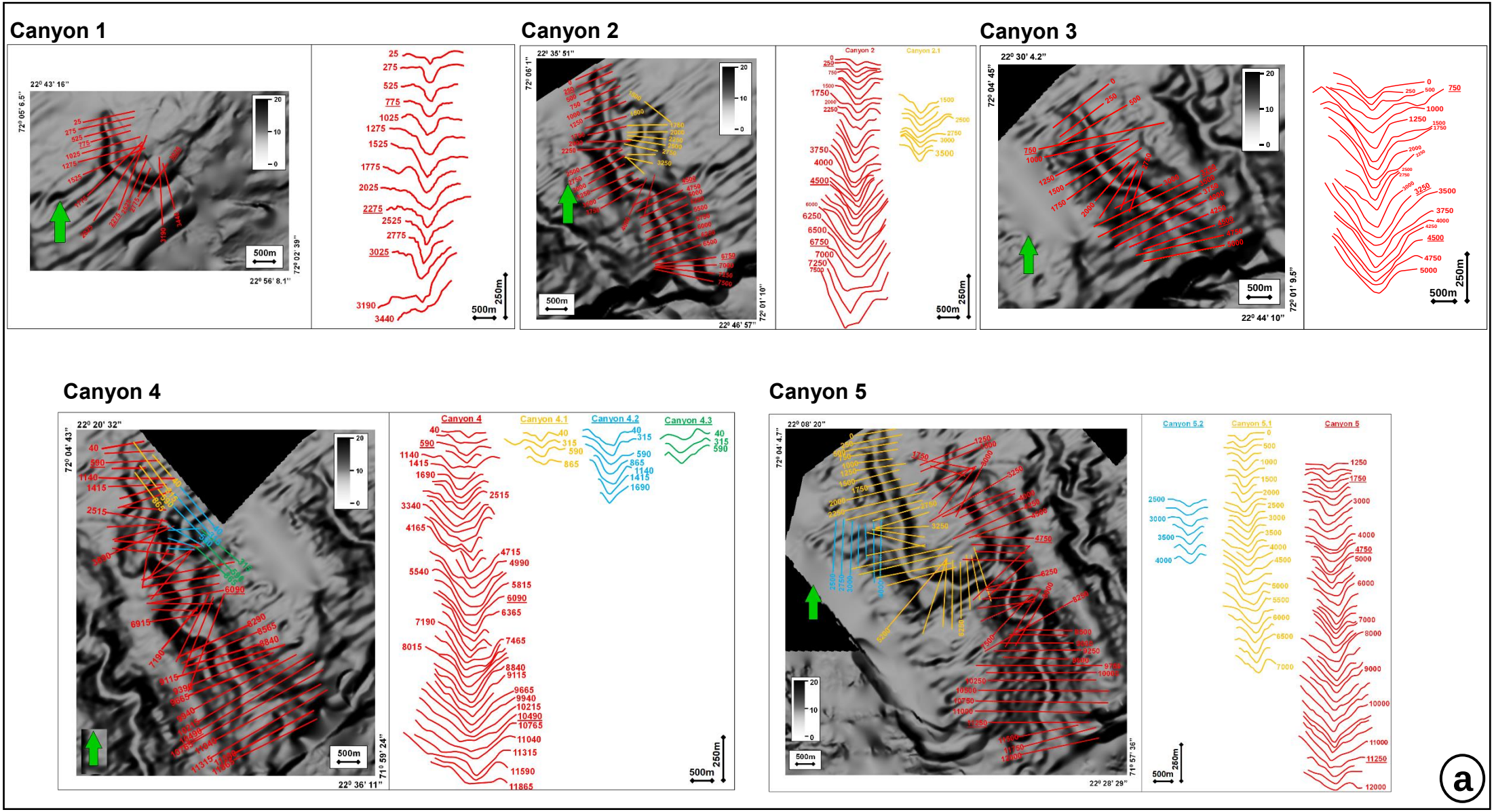

Figure 6. (Continued)

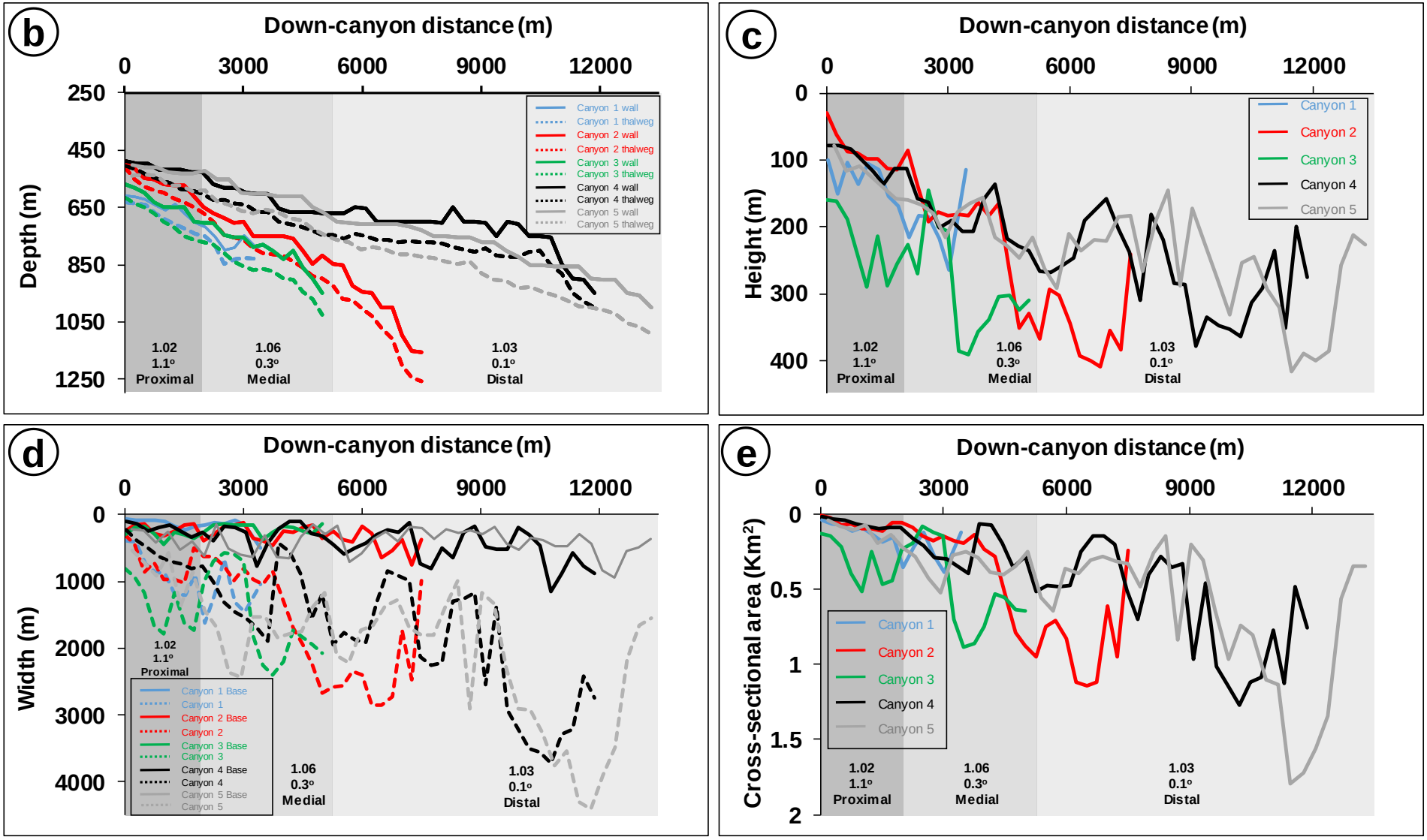

Figure 6. Morphometric analysis of canyons. (a) Dip angle (degrees) map of canyons, with locations of cross-sections (left images) and perpendicular canyon cross sections (right images). Notation is down-canyon distance. Underline notation is a section on the Figure 5. Red colour is the main canyon while the others are tributaries canyon. (b) Depth profile of canyon thalweg and canyon wall. (c) Canyon height profile. (d) Width of canyon and canyon base. (e) Cross-sectional area (CSA) of canyon. Average sinuosity index and canyon gradients (degrees) for each part of the canyon are at the bottom of the graphs. *See supplementary materials for individual canyon plots.*

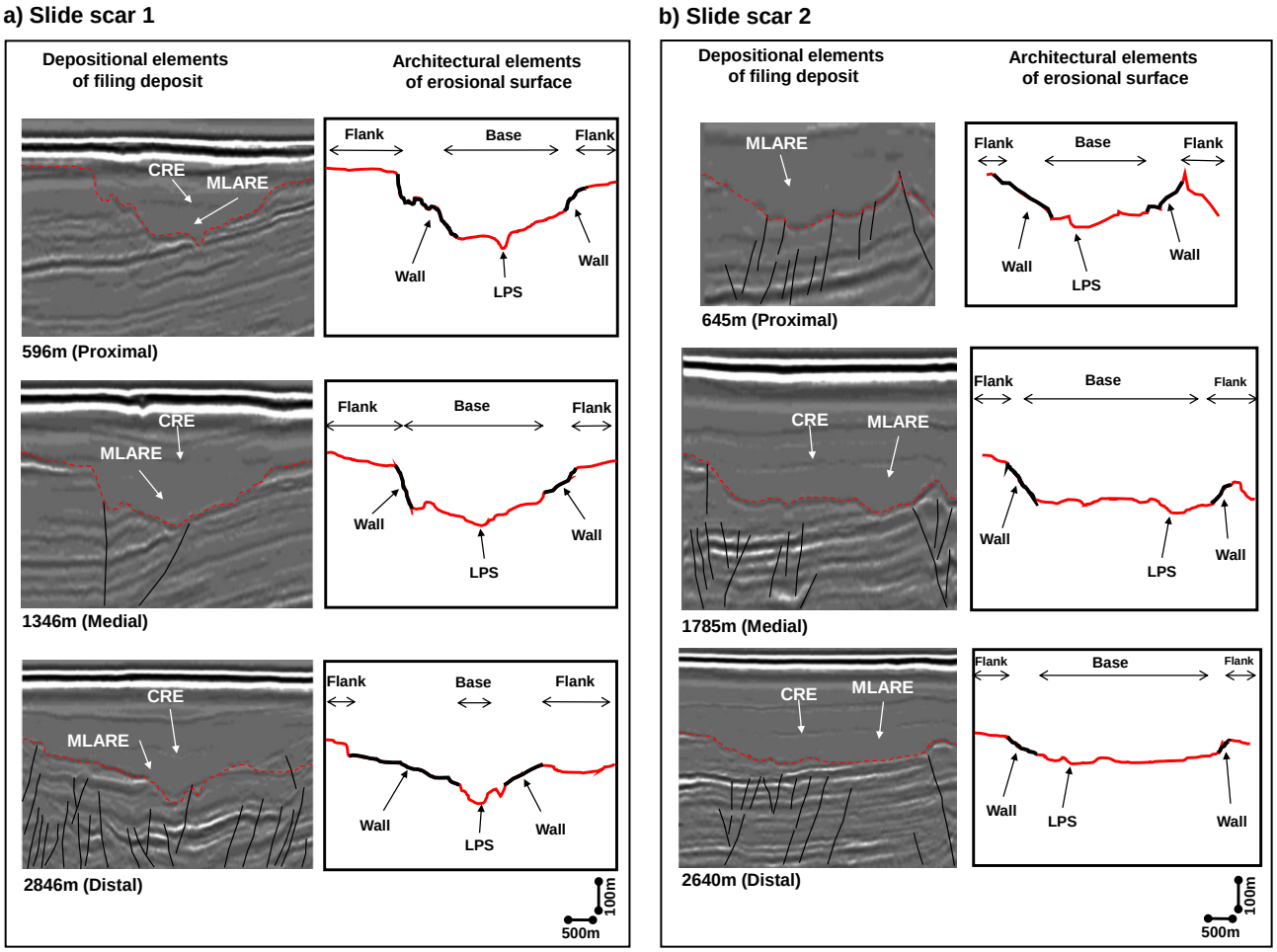

Figure 7. Seismic facies analysis of slide scars in the study area, representing the proximal – distal system. See Figure 8a for section location.

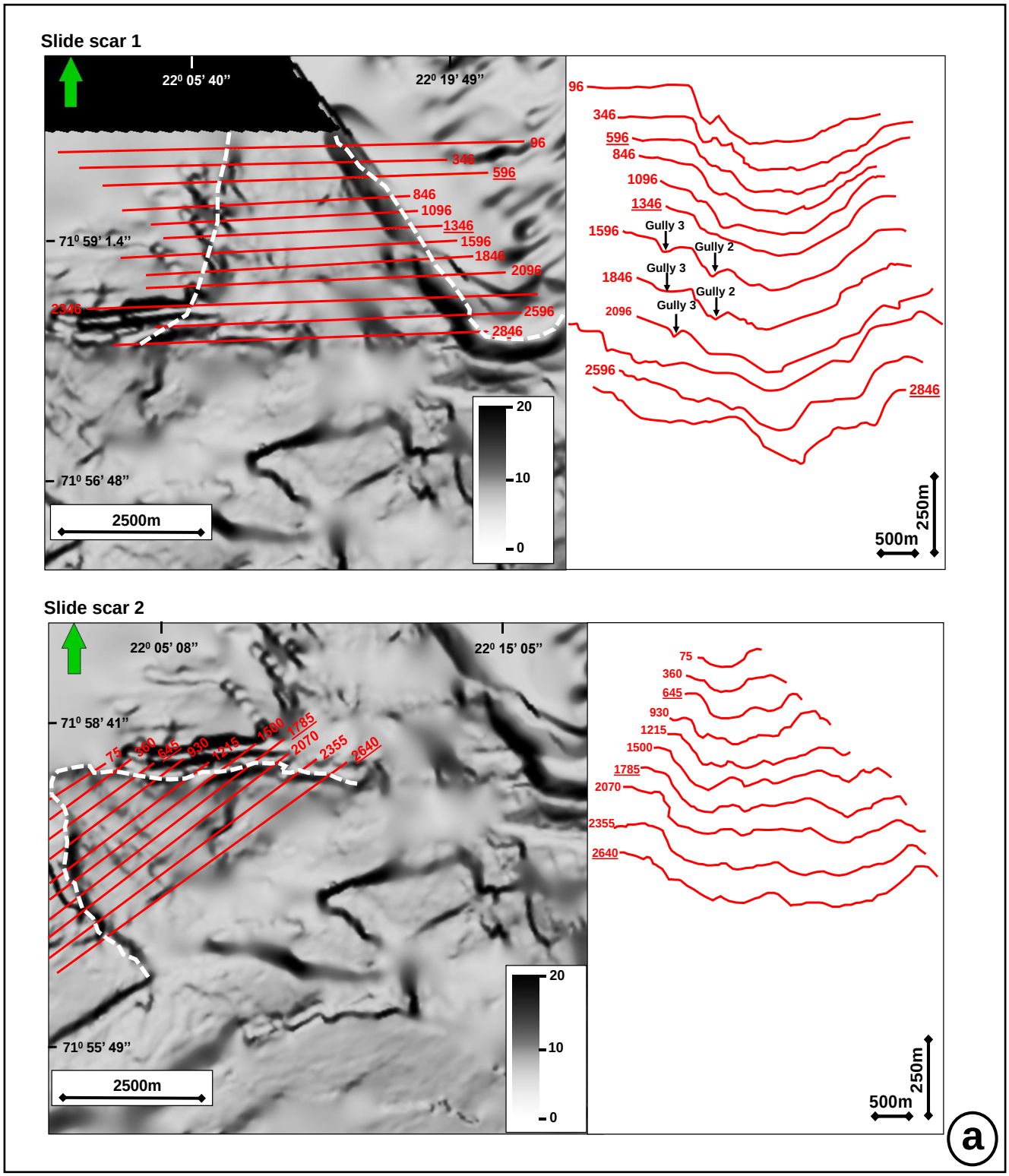

Figure 8. (Continued)

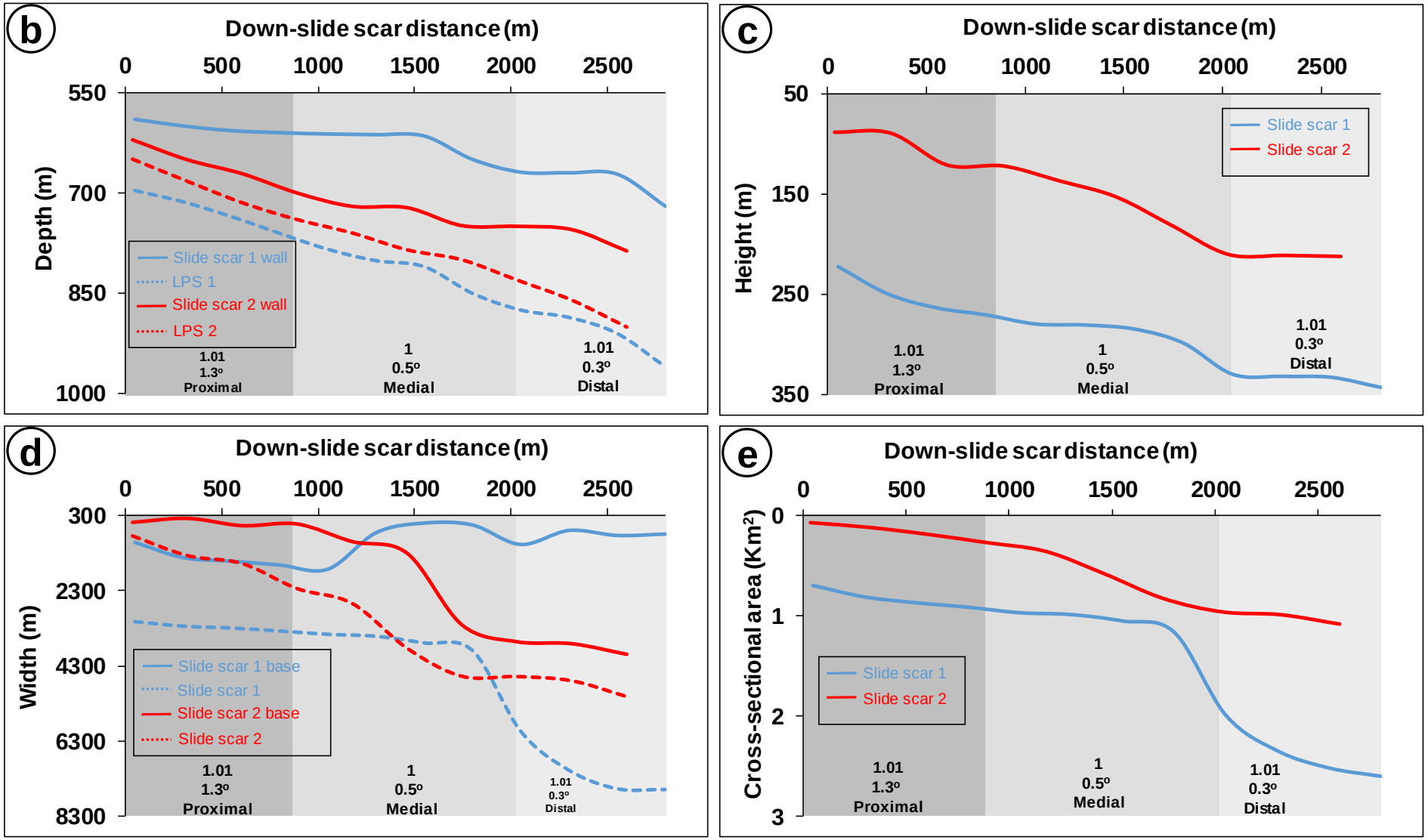

Figure 8. Morphometric analysis of Slide scar. (a) Dip angle (degrees) map of slide scar, with locations of cross-sections (Left images) and perpendicular slide scar cross sections (Right image). White dashed line is slide scar outline. Notation is down-slide scar distance. Underline notation is a section on the Figure 7. (b) Depth profile of the LPS and slide scar wall. (c) Slide scar height profile. (d) Width of slide scar and slide scar base. (e) Cross-sectional area (CSA) of slide scar. Average sinuosity index and slide scar gradients (degrees) for each part of the slide scar are at the bottom of the graphs. *See supplementary materials for individual slide scar plots.*

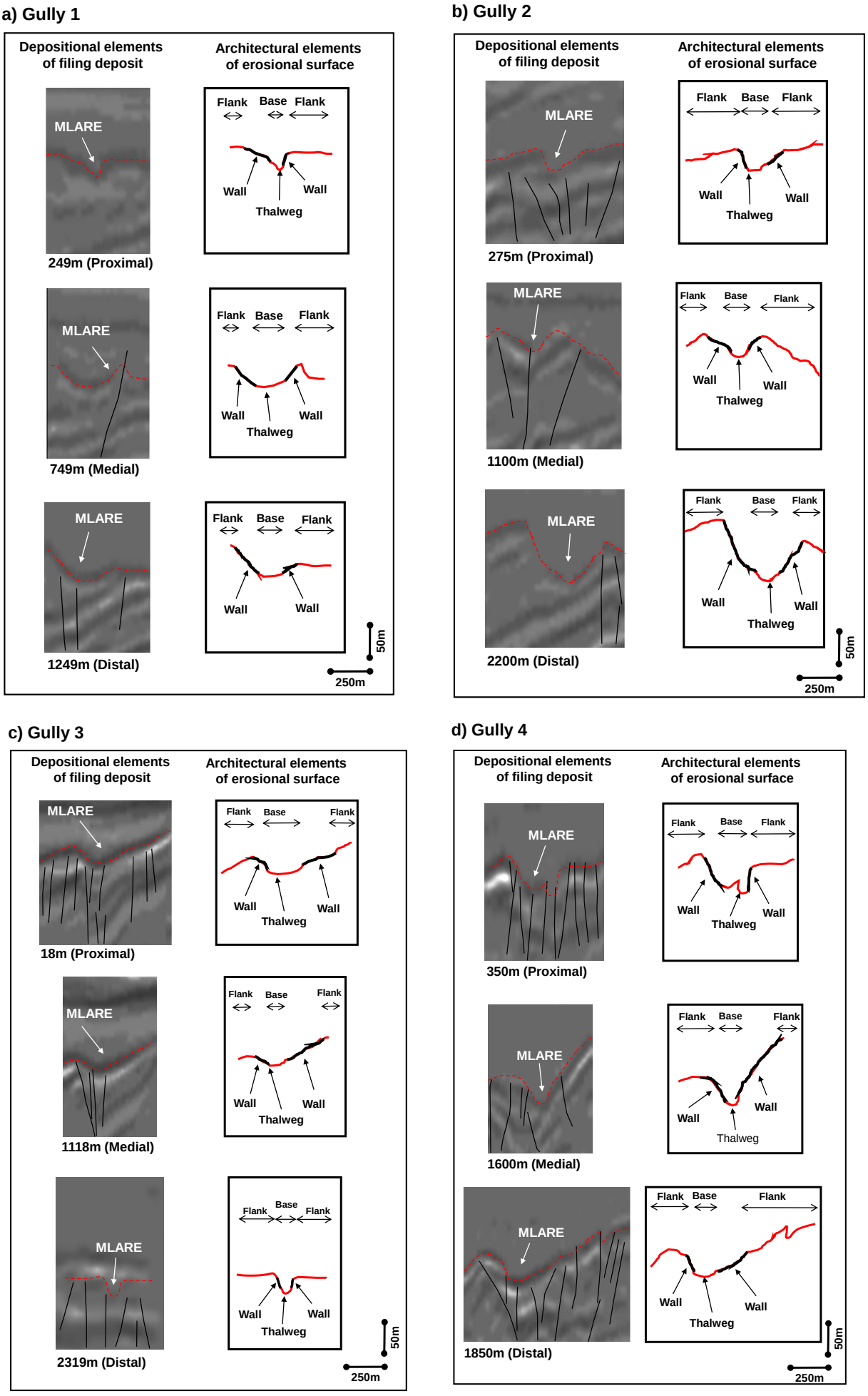

Figure 9. Seismic facies analysis of gullies in the study area, representing the proximal – distal system. See Figure 10a for section location.

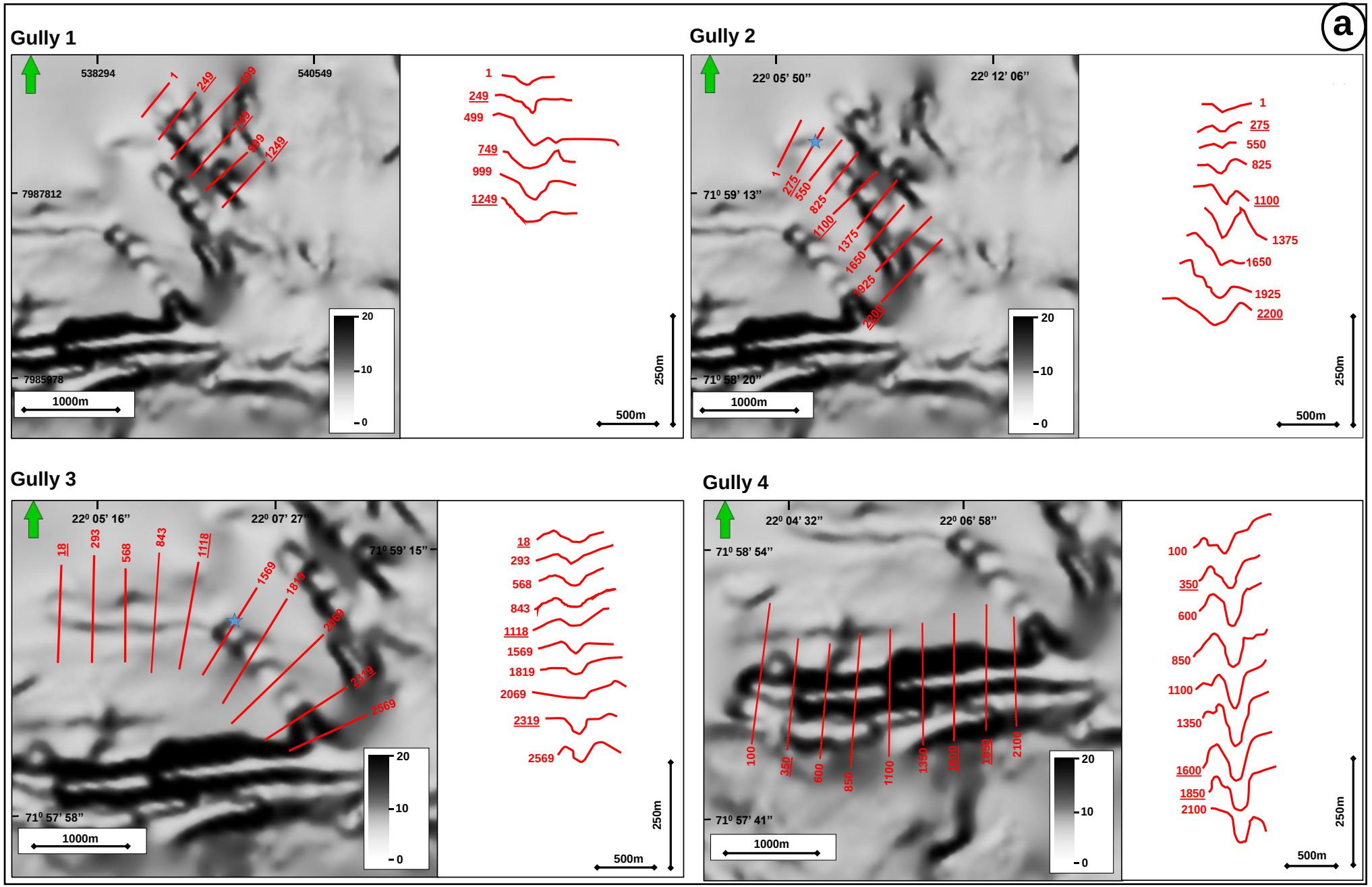

Figure 10. (Continued)

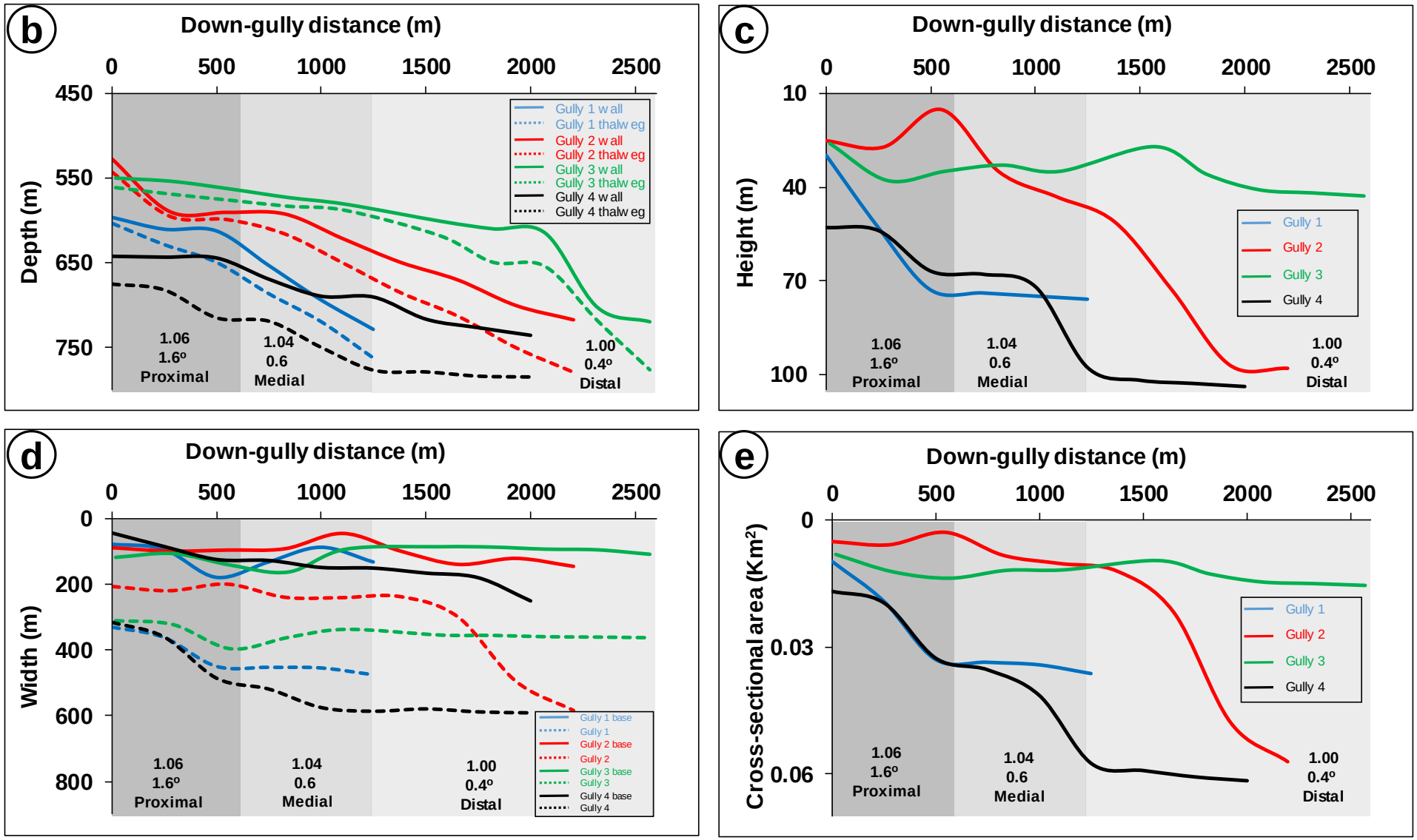

Figure 10. Morphometric analysis of gullies. (a) Dip angle (degrees) map of gullies, with locations of cross-sections (left images) and perpendicular gullies cross sections (right images). Blue star is knickpoint of gully. Notation is down-gully distance. Underline notation is a section on the Figure 9. (b) Depth profile of gully thalweg and gully walls. (c) Gully height profile. (d) Width of gullies and gully base. (e) Cross-sectional area of gullies. Average sinuosity index and gully gradients (degrees) for each part of the gully are at the bottom of the graphs. *See supplementary materials for individual gully plots.*

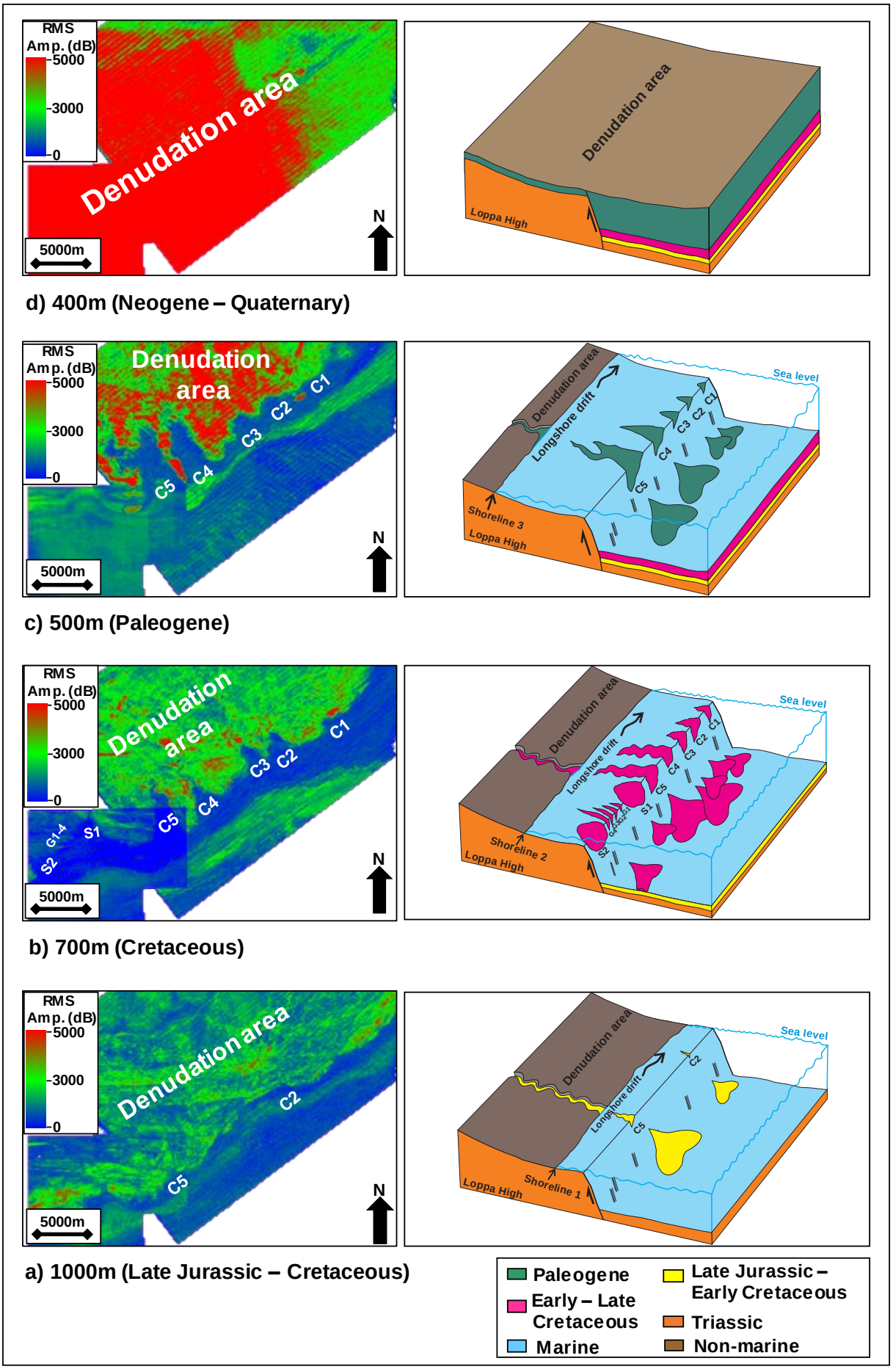

Figure 11. Evolution of sediment conduits in the SE Loppa High as represented by seismic depth slices of RMS Amplitude (left image), and its schematic model (right image). *C denotes Canyon; S denotes Slide, and G denotes Gully.*

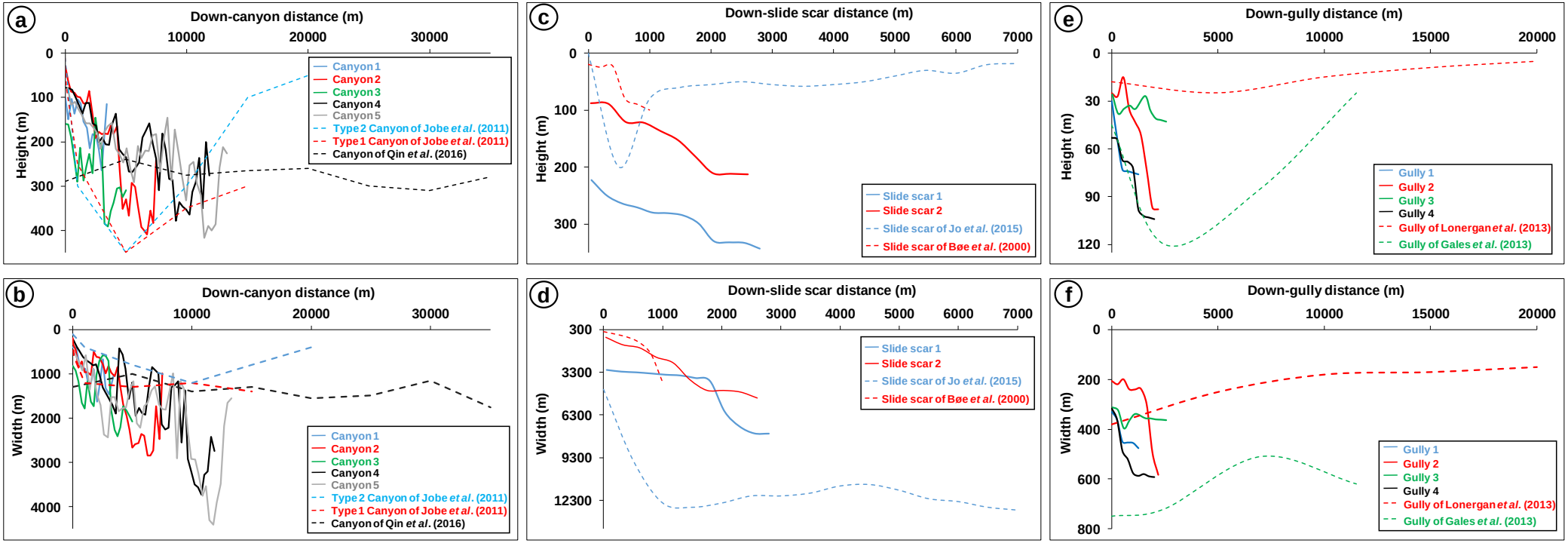

Figure 12. Morphometry comparison of sediment conduits on the study area with Jobe *et al.* (2011) and Qin *et al.* (2016) on the canyon system, Jo *et al.* (2015) and Bøe *et al.* (2000) on the slide scar system, Lonergan *et al.* (2013) and Gales *et al.* (2013) on the gully system.

Morphometric plots of sediment conduits on a bathymetric high: implications for paleoenvironment and hydrocarbon prospectivity

Dicky Harishidayat, Kamaldeen Olakunle Omosanya, Ståle Emil Johansen, Ovie Emmanuel Eruteya, Yakufu Niyazi

Supplementary Materials

Contents:

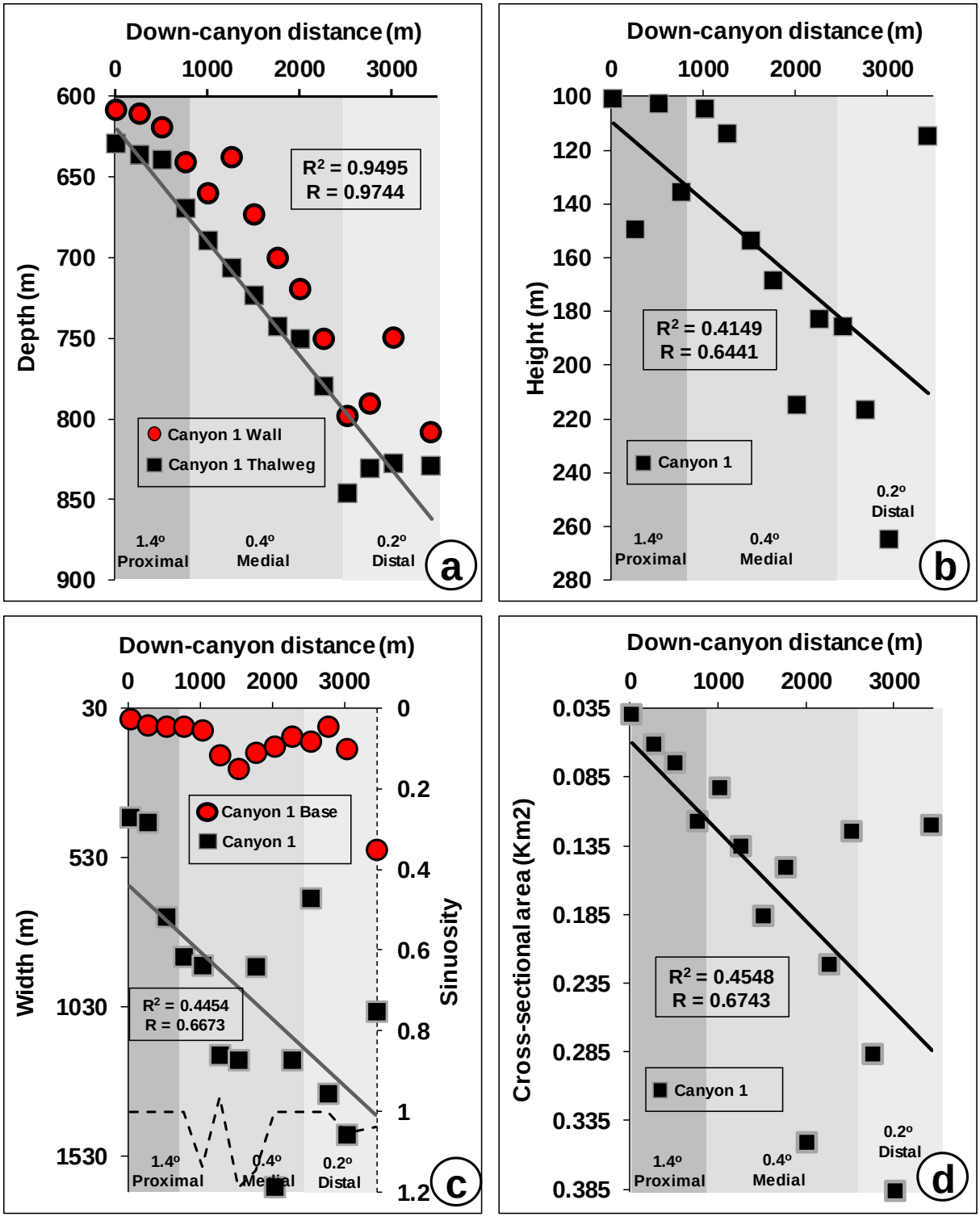

Figure S1. Morphometric plots for Canyon 1. (a) Depth profile of canyon thalweg and canyon wall. (b) Canyon height profile. (c) Sinuosity of the canyon (Dashed line) together with width of canyon and canyon base. (d) Cross-sectional area of canyon. Average canyon gradients (degree) for each part of the canyon are at the bottom of the graphs.

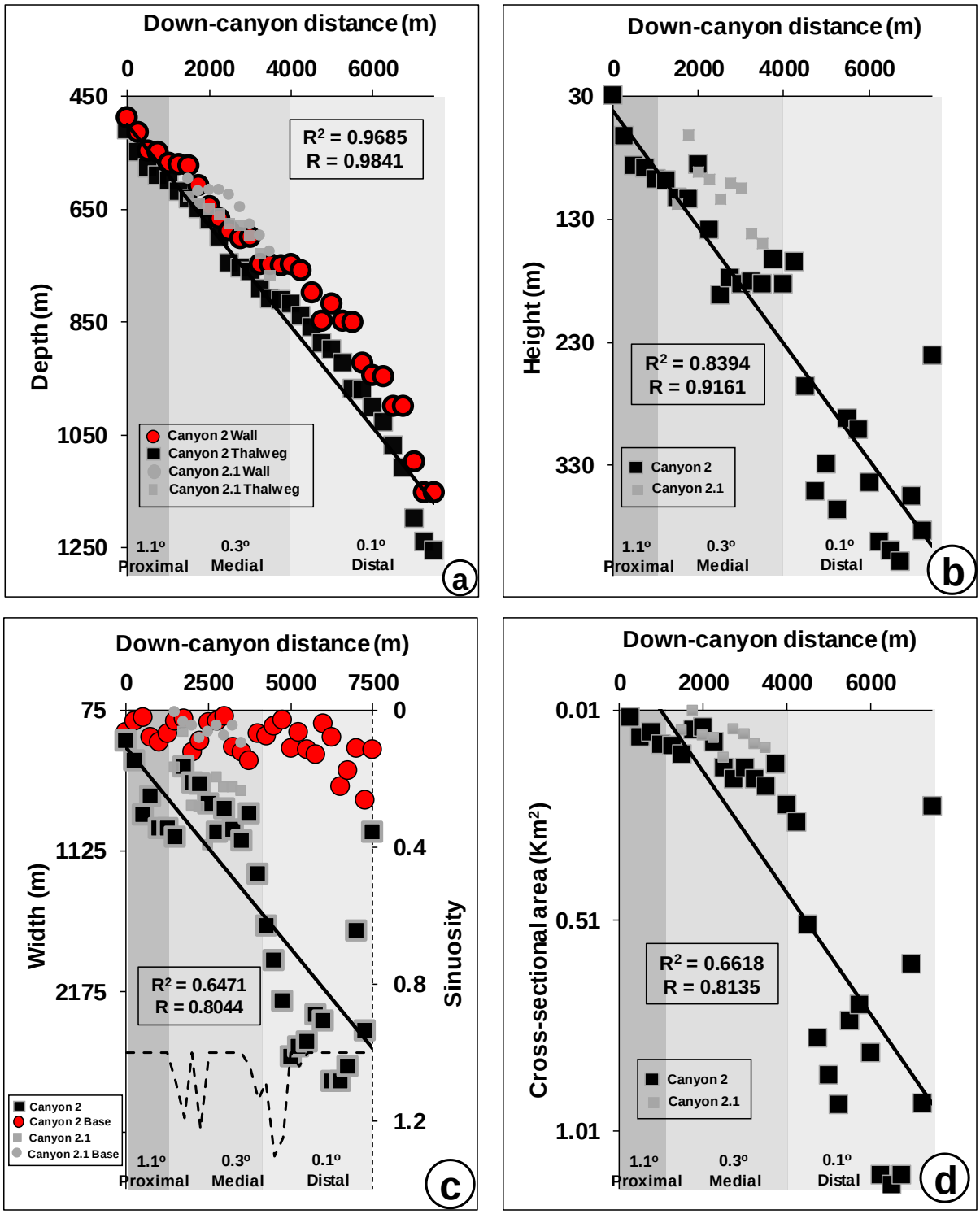

Figure S2. Morphometric plots for Canyon 2. (a) Depth profile of canyon thalweg and canyon wall. (b) Canyon height profile. (c) Sinuosity of the canyon (Dashed line) together with width of canyon and canyon base. (d) Cross-sectional area of canyon. Average canyon gradients (degree) for each part of the canyon are at the bottom of the graphs. *Tributary canyons represented by small symbols.*

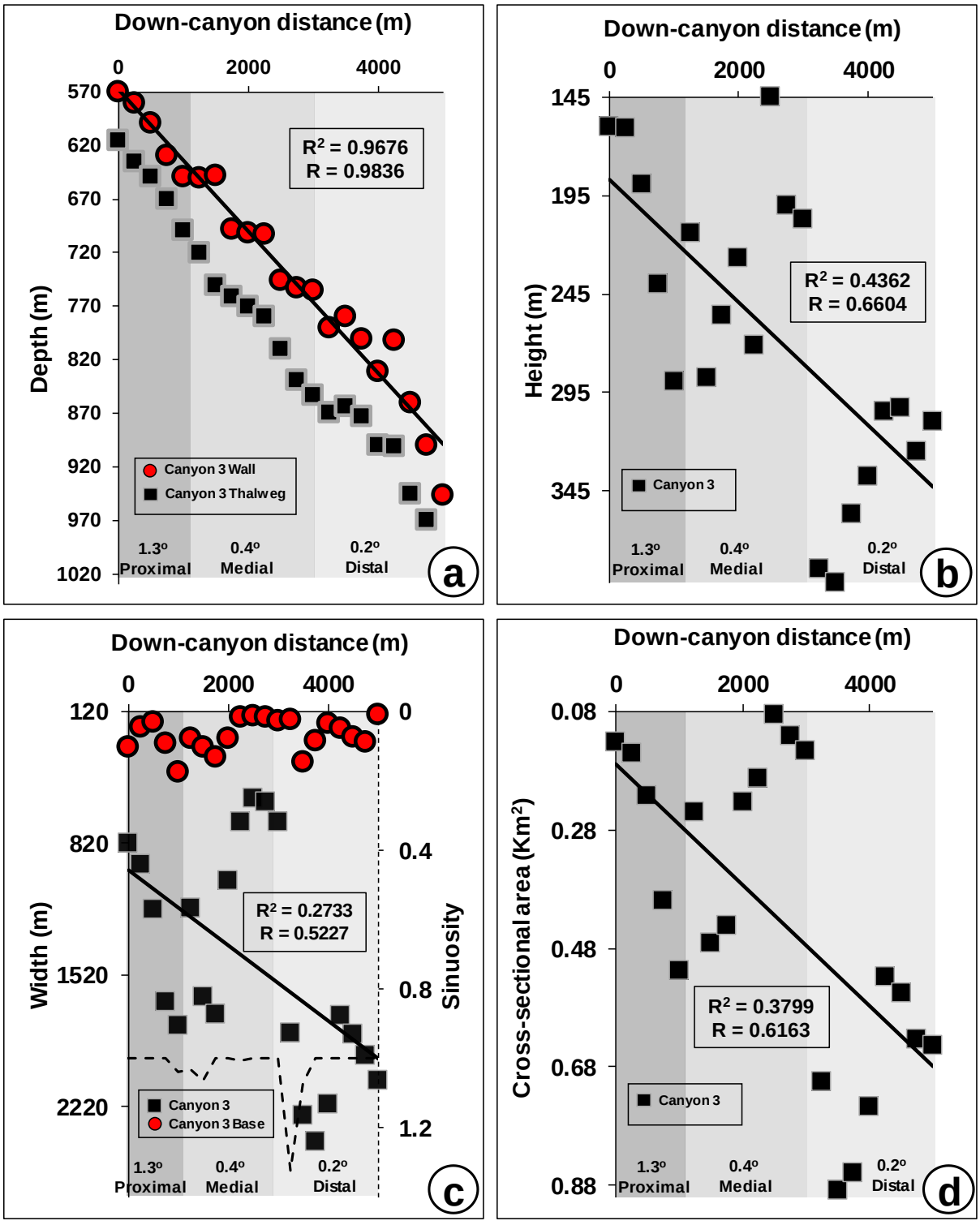

Figure S3. Morphometric plots for Canyon 3. (a) Depth profile of canyon thalweg and canyon wall. (b) Canyon height profile. (c) Sinuosity of the canyon (Dashed line) together with width of canyon and canyon base. (d) Cross-sectional area of canyon. Average canyon gradients (degree) for each part of the canyon are at the bottom of the graphs.

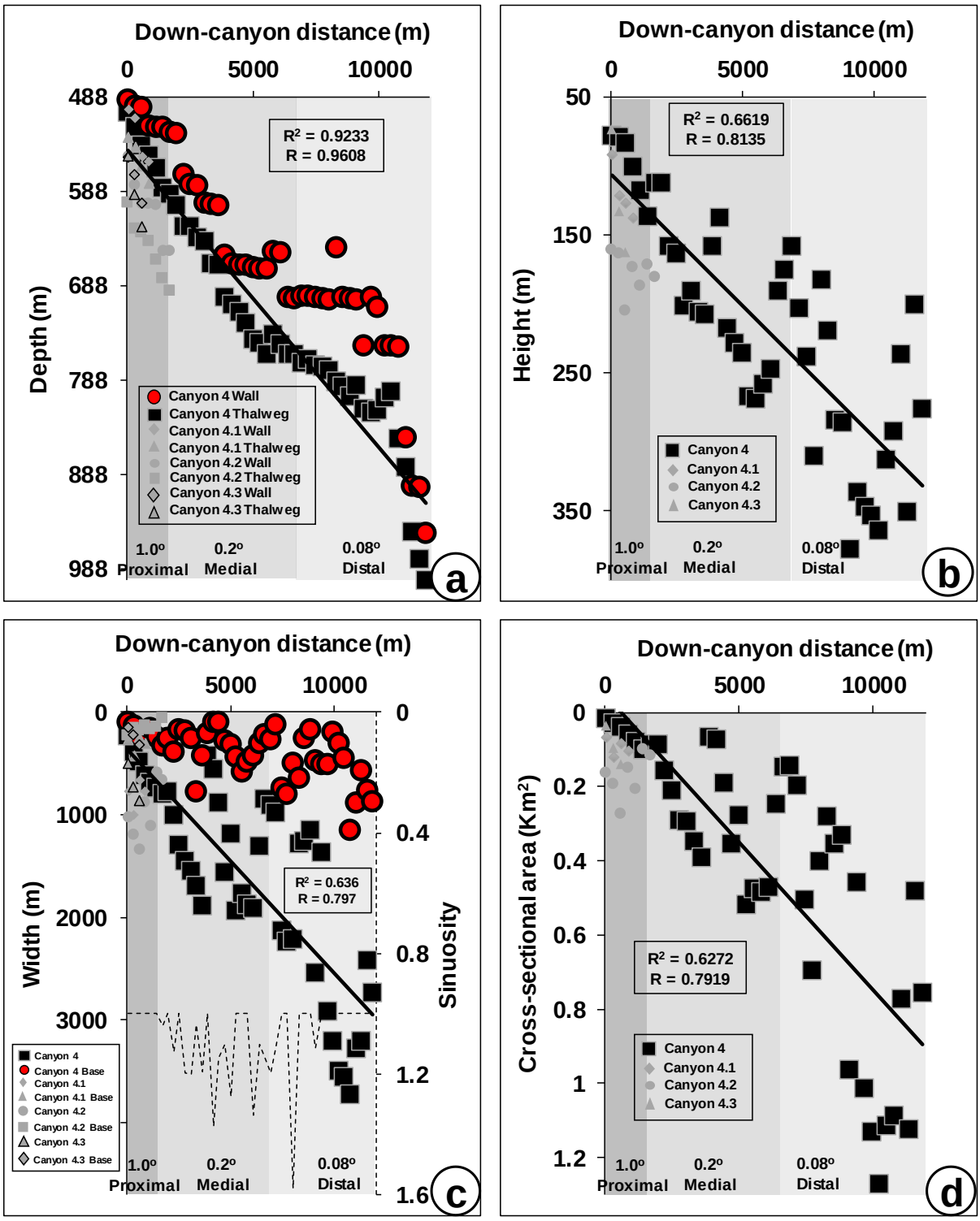

Figure S4. Morphometric plots for Canyon 4. (a) Depth profile of canyon thalweg and canyon wall. (b) Canyon height profile. (c) Sinuosity of the canyon (Dashed line) together with width of canyon and canyon base. (d) Cross-sectional area of canyon. Average canyon gradients (degree) for each part of the canyon are at the bottom of the graphs. *Tributary canyons represented by small symbols.*

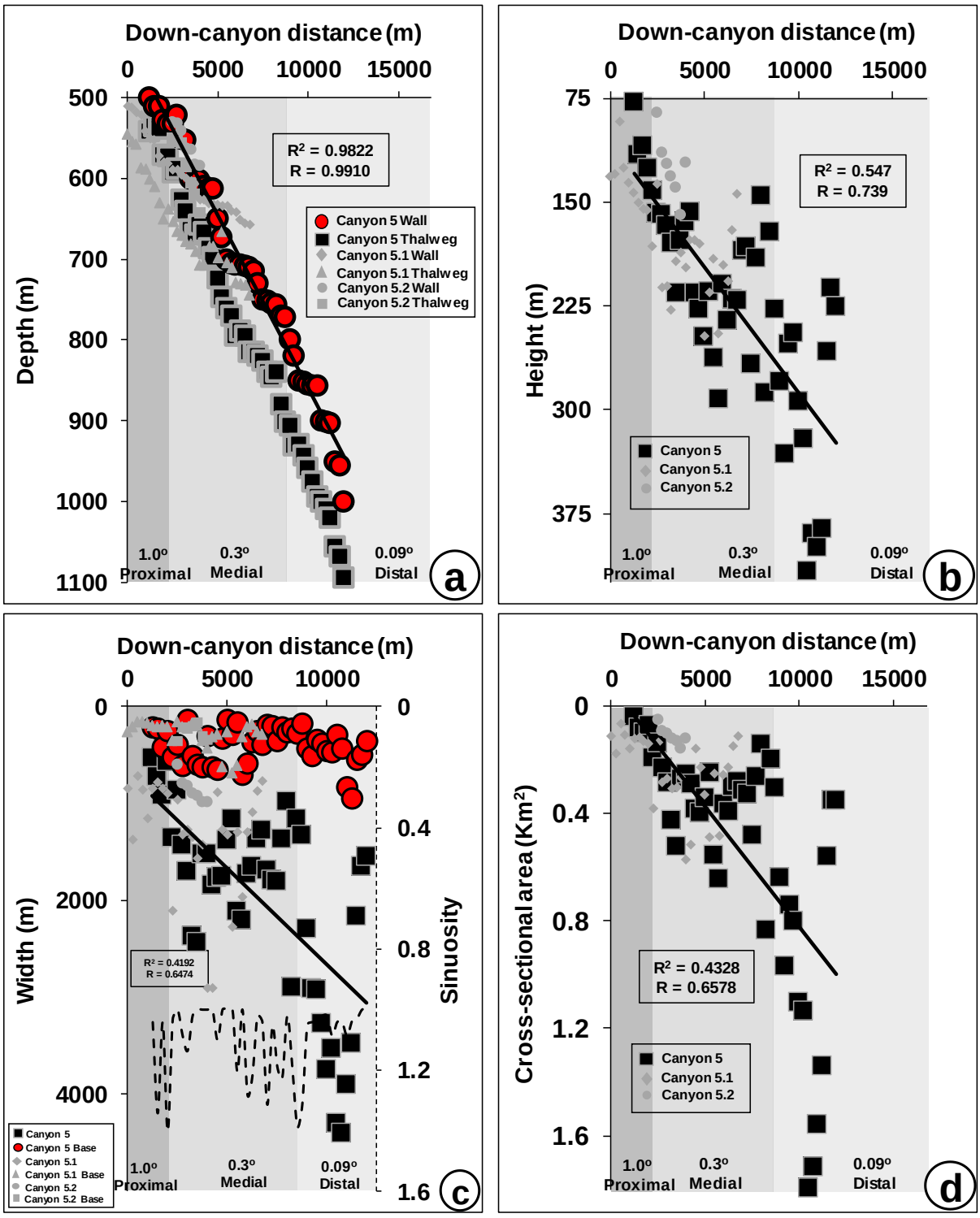

Figure S5. Morphometric plots for Canyon 5. (a) Depth profile of canyon thalweg and canyon wall. (b) Canyon height profile. (c) Sinuosity of the canyon (Dashed line) together with width of canyon and canyon base. (d) Cross-sectional area of canyon. Average canyon gradients (degree) for each part of the canyon are at the bottom of the graphs. *Tributary canyons represented by small symbols.*

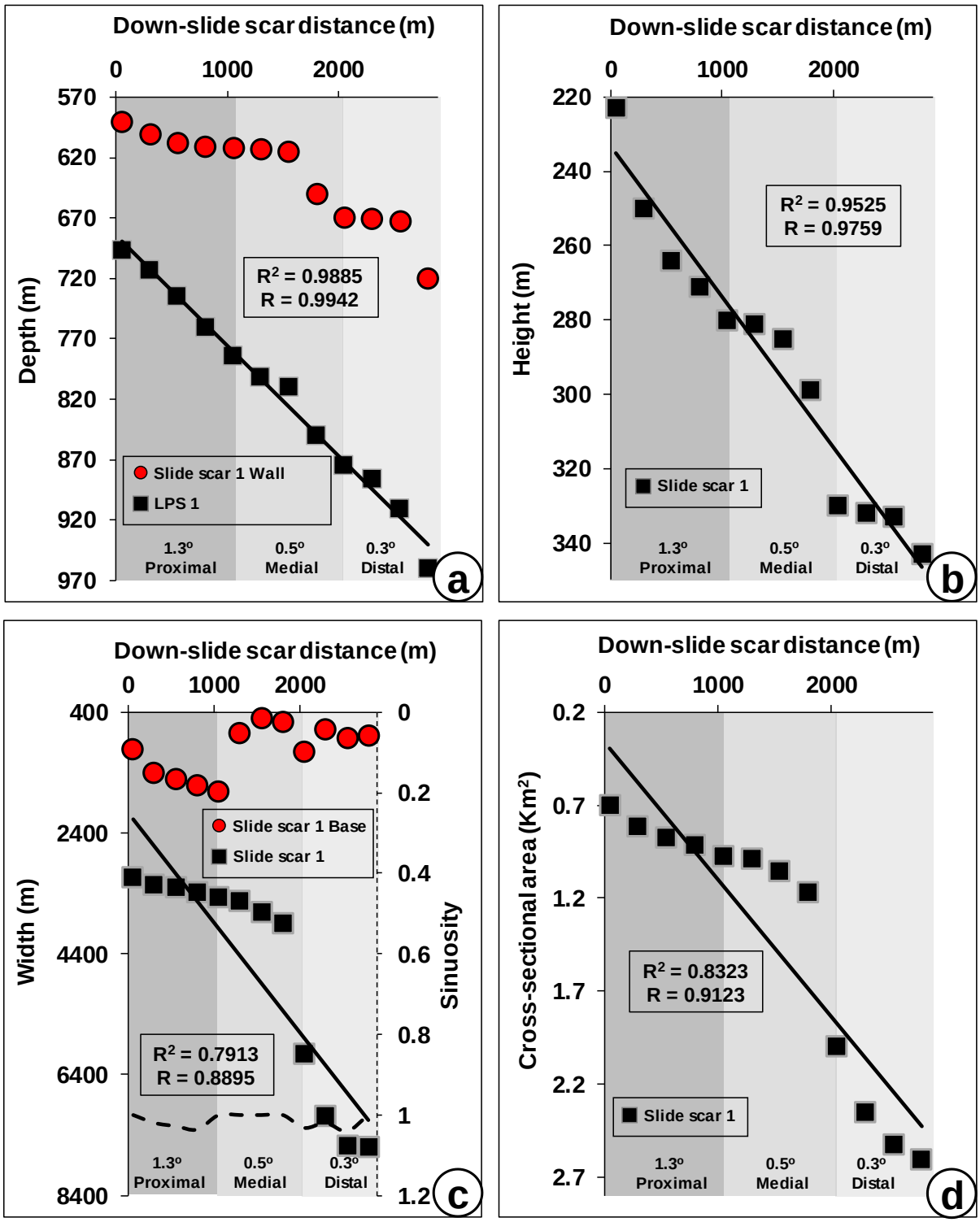

Figure S6. Morphometric plots for Slide scar 1. (a) Depth profile of slide scar wall and the LPS. (b) Slide scar height profile. (c) Sinuosity of slide scar (dashed line) together with width of slide scar and slide scar base. (d) Cross-sectional area of slide scar. Average slide scar gradients (degree) for each part of the slide scar are at the bottom of the graphs.

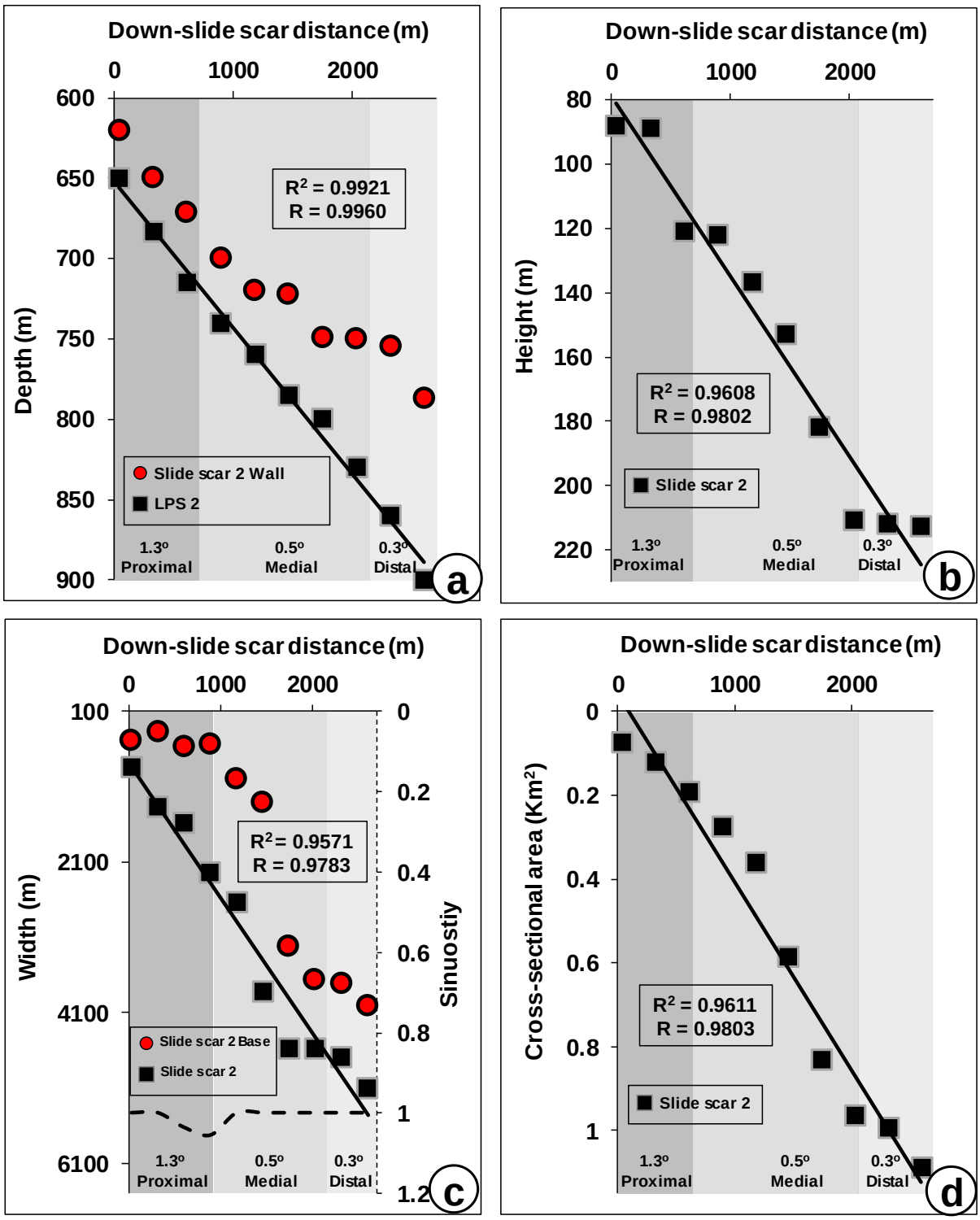

Figure S7. Morphometric plots for Slide scar 2. (a) Depth profile of slide scar wall and the LPS. (b) Slide scar height profile. (c) Sinuosity of slide scar (dashed line) together with width of slide scar and slide scar base. (d) Cross-sectional area of slide scar. Average slide scar gradients (degree) for each part of the slide scar are at the bottom of the graphs.

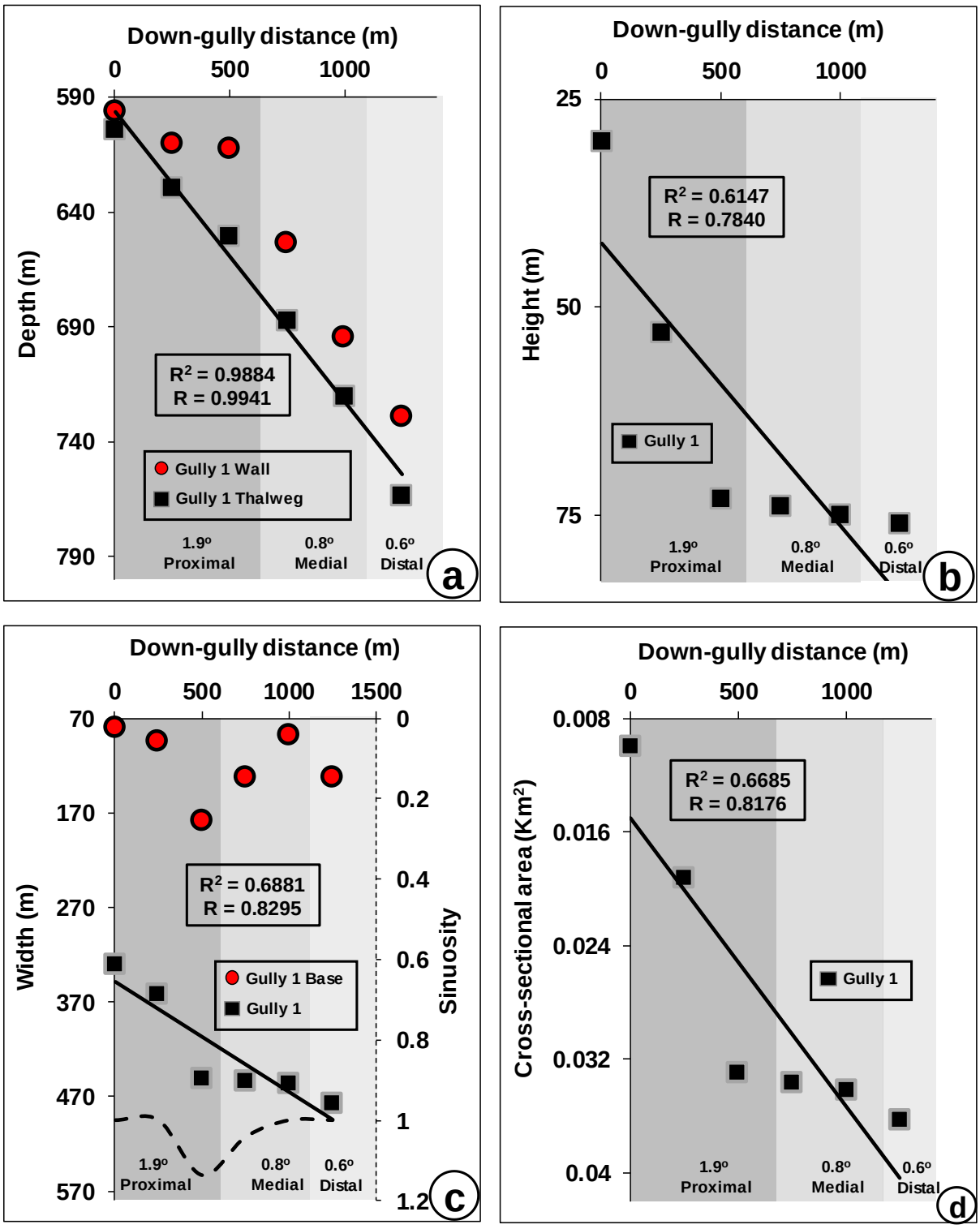

Figure S8. Morphometric plots for Gully 1. (a) Depth profile of gully thalweg and gully wall. (b) Gully height profile. (c) Sinuosity of gully (dashed line) together with width of gully and gully base. (d) Cross-sectional area of gully. Average gully gradients (degree) for each part of the gully are at the bottom of the graphs.

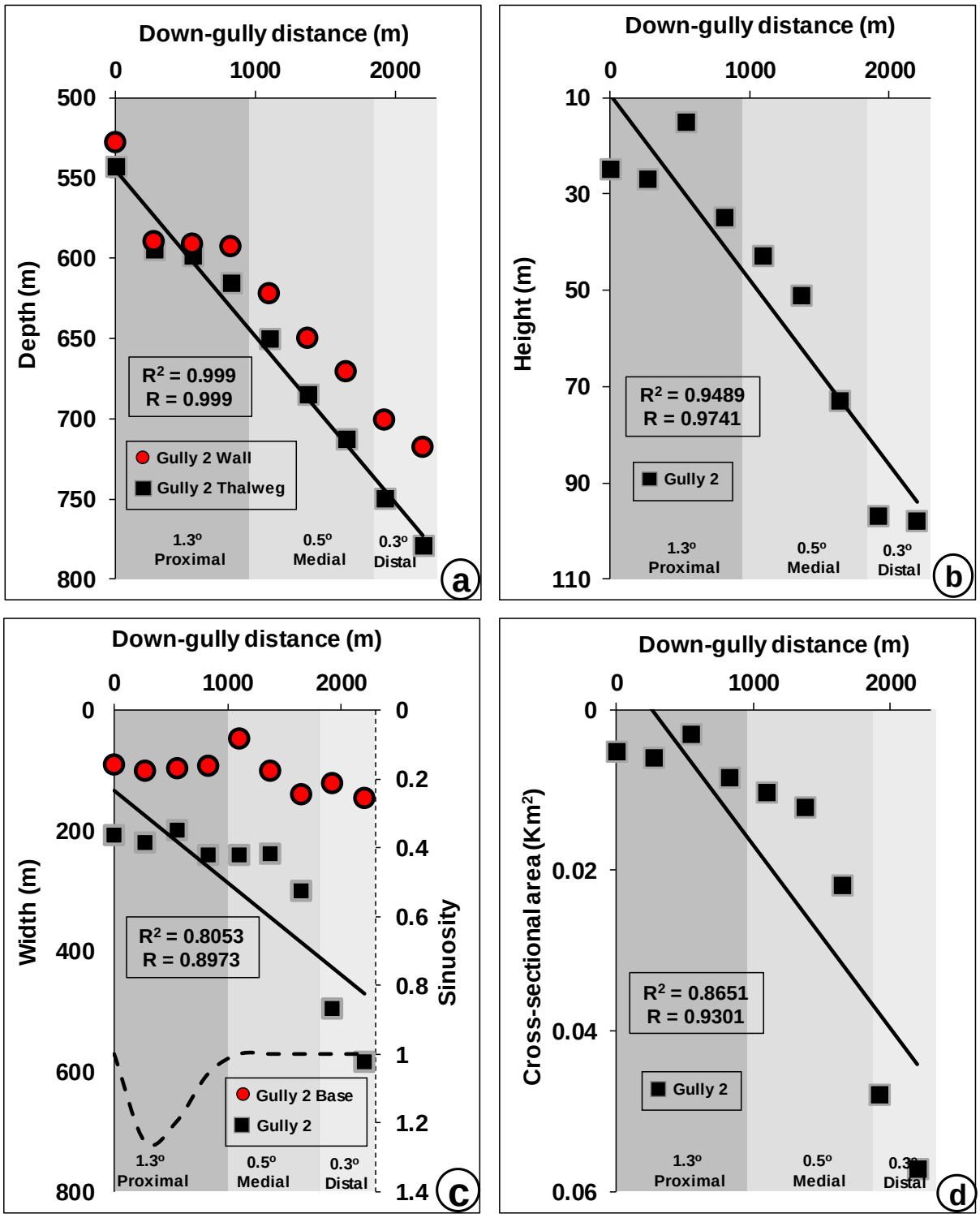

Figure S9. Morphometric plots for Gully 2. (a) Depth profile of gully thalweg and gully wall. (b) Gully height profile. (c) Sinuosity of gully (dashed line) together with width of gully and gully base. (d) Cross-sectional area of gully. Average gully gradients (degree) for each part of the gully are at the bottom of the graphs.

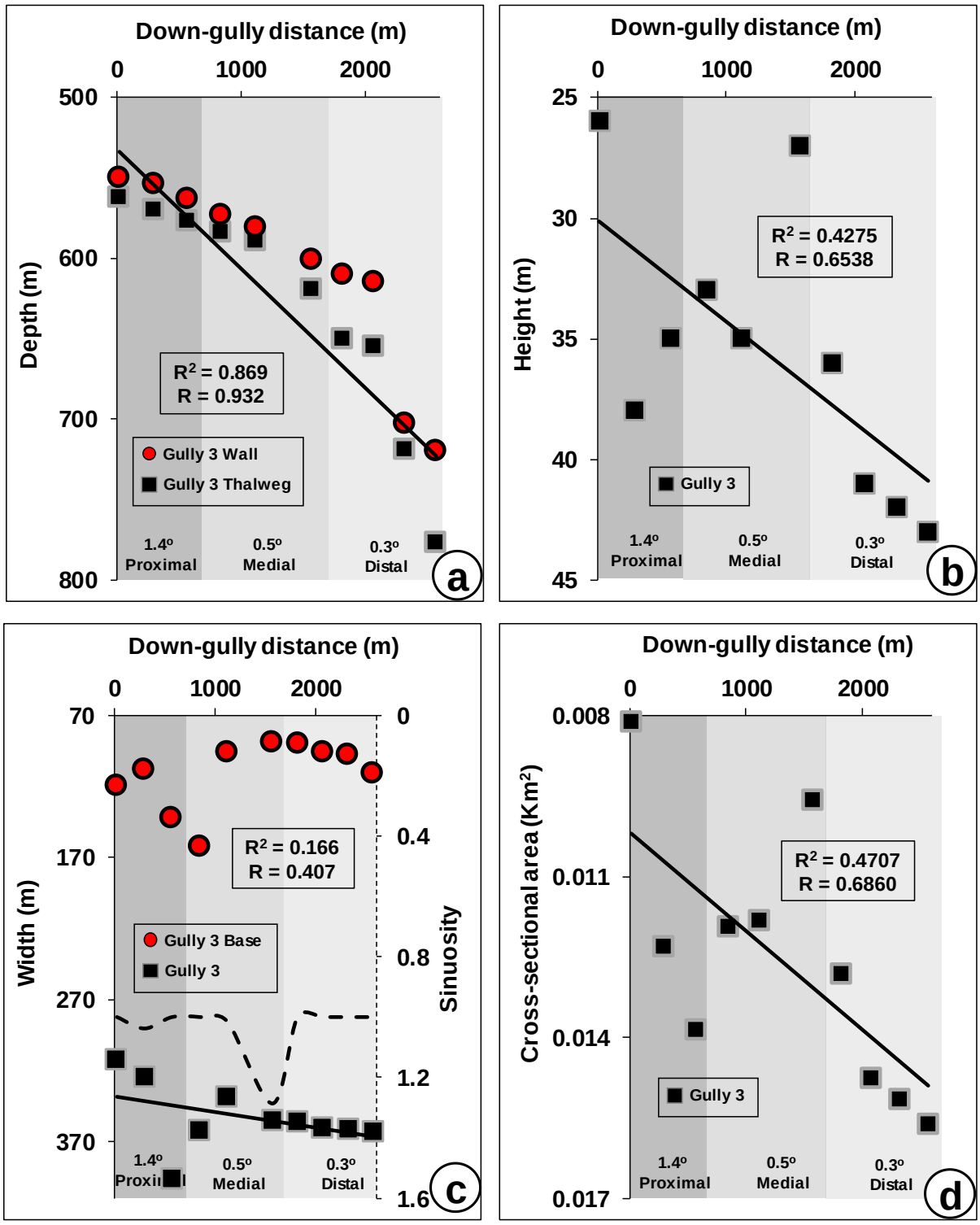

Figure S10. Morphometric plots for Gully 3. (a) Depth profile of gully thalweg and gully wall. (b) Gully height profile. (c) Sinuosity of gully (dashed line) together with width of gully and gully base. (d) Cross-sectional area of gully. Average gully gradients (degree) for each part of the gully are at the bottom of the graphs.

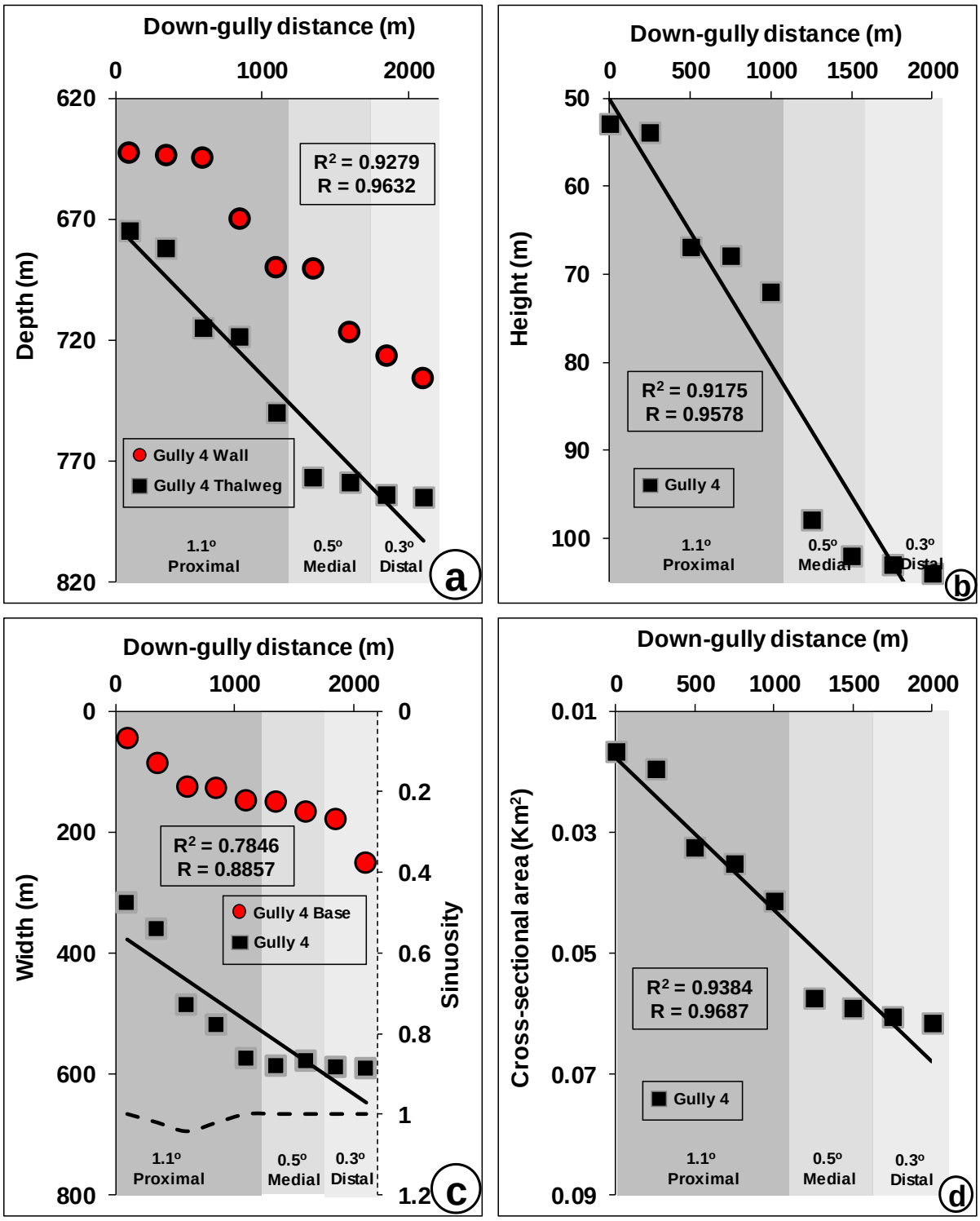

Figure S11. Morphometric plots of Gully 4. (a) Depth profile of gully thalweg and gully wall. (b) Gully height profile. (c) Sinuosity of gully (dashed line) together with width of gully and gully base. (d) Cross-sectional area of gully. Average gully gradients (degree) for each part of the gully are at the bottom of the graphs.